Am J Cancer Res 2024;14(7):3294-3316
www.ajcr.us /ISSN:2156-6976/ajcr0156965

*Original Article*

# STAC3 as a poor prognostic biomarker in renal clear cell carcinoma: relationship with immune infiltration

Yingnan Zhang*, Jingtao Li*, Luwen Feng*, Yue Cheng, Linlin Shi, Qian Yang, Zhaoyang Wang, Xuan Yi, Guocai Zhong, Xueying Sun, Zhifeng Cheng, Min Guo

*The Fourth Affiliated Hospital of Harbin Medical University, Harbin 150001, Heilongjiang, China. *Equal contributors.*

Received April 2, 2024; Accepted June 17, 2024; Epub July 15, 2024; Published July 30, 2024

**Abstract:** Calcium ions ($Ca^{2+}$) are crucial in tumorigenesis and progression, with their elevated levels indicating a negative prognosis in Kidney Renal Clear Cell Carcinoma (KIRC). The influence of genes regulating calcium ions on the survival outcomes of KIRC patients and their interaction with the tumor's immune microenvironment is yet to be fully understood. This study analyzed gene expression data from KIRC tumor and adjacent non-tumor tissues using the TCGA-KIRC dataset to pinpoint genes that are differentially expressed in KIRC. Intersection of these genes with those regulating calcium ions highlighted specific calcium ion-regulating genes that exhibit differential expression in KIRC. Subsequently, prognostic risk models were developed using univariate Cox and LASSO-Cox regression analyses to verify their diagnostic precision. Additionally, the study investigated the correlation between tumor immunity and KIRC patient outcomes, assessing the contribution of STAC3 genes to tumor immunity. Further exploration entailed SSGASE, single-cell analysis, pseudotime analysis and both in vivo and in vitro experiments to evaluate STAC3's role in tumor immunity and progression. Notably, STAC3 was significantly overexpressed in tumor specimens and positively correlated with the degree of malignancy of KIRC, affecting patients' prognosis. Elevated STAC3 expression correlated with enhanced immune infiltration in KIRC tumors. Furthermore, silencing STAC3 curtailed KIRC cell proliferation, migration, invasion, and stemness properties. Experimental models in mice confirmed that STAC3 knockdown led to a reduction in tumor growth. Elevated STAC3 expression is intricately linked with immune infiltration in KIRC tumors, as well as with the aggressive biological behaviors of tumor cells, including their proliferation, migration, and invasion. Targeting STAC3 presents a promising strategy to augment the efficacy of current therapeutic approaches and to better the survival outcomes of patients with KIRC.

**Keywords:** Kidney renal clear cell carcinoma, prognostic risk model, tumor immune, STAC3

## Introduction

Renal cell carcinoma (RCC), a significant global health concern, is predominantly comprised of KIRC, constituting the majority of RCC cases at over 70% [1, 2]. KIRC is identified as the 13th leading cause of cancer death globally, as per the World Health Organization's recent data [3, 4].

In clinical practice, a substantial number of KIRC patients experience severe side effects from conventional treatments like chemotherapy, radiotherapy, or targeted therapy, often making surgical resection the preferable treatment option [5, 6]. However, about 30% of patients face recurrence or metastasis post-nephrectomy, with metastatic KIRC being almost invariably fatal and having a 10-year survival rate below 5% [7]. Given the heterogeneity of KIRC, effective molecular markers are necessary for personalized treatment strategies. Identifying biomarkers is key for optimizing treatment choices, reducing costs, and enhancing survival rates in KIRC patients.

$Ca^{2+}$ plays a pivotal role in tumor development, serving as a versatile signaling tool in tumor cells, such as proliferation, invasion, and sensitivity to cell death [8-11]. Alterations in the expression of proteins directly involved in $Ca^{2+}$ signaling are not only regulators of oncogenic signaling but may also initiate certain cancers [11].

https://doi.org/10.62347/EAQW3113

Cells from both adaptive and innate immune systems intermingle within the tumor microenvironment (TME) of KIRC, forming a complex ecosystem that plays a pivotal role in tumor development [1, 3, 12, 13]. This dynamic TME, varying by tumor type, is composed mainly of stromal cells, immune cells, and the extracellular matrix (ECM), with immune cells being a critical component [14-16]. In renal cancer, the TME is particularly active in facilitating immune evasion [17]. KIRC is distinct in its TME, characterized by a high degree of immune cell infiltration, particularly T cells. T cells and tumor-associated macrophages (TAMs) are the primary immune populations in KIRC, representing 51% and 31%, respectively [18-20]. Most CD8+ T cells in this environment are exhausted and functionally impaired [16]. Emerging research indicates a strong connection between the efficacy of immune checkpoint inhibitors (ICIs) and the TME's composition, underscoring the importance of understanding KIRC's TME and its related genetic factors in disease progression and treatment [21, 22].

STAC3 is a member of the Stac gene family and contains an N-terminal cysteine-rich domain and two SH3 domains [23, 24]. Research shows that STAC3 is a component of the muscle excitation-contraction coupling mechanism and plays an important role in calcium regulation mechanisms [25, 26]. STAC3 has been found to interact with RNA methylation modifications, such as m6A, m5C, and m1A, in cervical cancer [27]. Existing research has demonstrated that STAC3 can interact with CaV1.1 through two distinct interactions [28-30]. One interaction occurs between the CaV1.1 II-III loop and the SH3 domain of STAC3, and the other interaction is between the C-terminal of CaV1.1 and the linker region of STAC3 [26, 29]. These interactions allow STAC3 to stabilize the slow kinetics of CaV1.1 currents, establishing STAC3 as a key determinant of the characteristically slow activation kinetics of CaV1.1 currents [30]. Additionally, STAC3 as a surface marker of macrophages affects the prognosis of renal clear cell carcinoma, but the specific mechanisms are not yet fully described [18].

Considering the significant heterogeneity of $Ca^{2+}$ regulatory genes and TME in KIRC, it is essential to comprehend their effects on the TME and their prognostic value in KIRC [11, 31]. Hence, we have constructed a clinical predictive model centered on $Ca^{2+}$ regulatory genes. STAC3 as a pivotal gene notably influences immune cell infiltration and tumor progression in KIRC's TME, laying a molecular groundwork for understanding KIRC's pathogenesis and therapeutic strategies. The flow chart of the study is shown in **Figure 1**.

## Materials and methods

### *Clinical tissue specimens*

In this study, we randomly selected samples included 40 anonymized patients who had both clinical data and paired non-cancerous tissue samples, which were obtained from the Fourth Affiliated Hospital of Harbin Medical University. Ethical approval for the study was secured from the Institutional Review Board of the aforementioned hospital.

### *Cell lines*

The KIRC cell lines 769-P and Caki-1, procured from the American Type Culture Collection (ATCC), were cultured in 1640 medium. These cells were maintained in a humidified 37°C incubator with a 5% $CO_2$ atmosphere. Culture media, enriched with 10% fetal bovine serum (FBS, 164210-50, Procell) and 1% antibiotic mixture (penicillin and streptomycin, PB180120, Procell), supported cell growth. To confirm the cell lines' authenticity and reduce misidentification, short tandem repeat profiling was utilized for cell line authentication.

### *Lentiviral transfection*

Lentiviral particles for STAC3 knockdown, designated as sh-STAC3, were acquired from JiKai Gene Technologies Co., Ltd., China, specifically targeting the STAC3 gene. The non-targeting control was termed NC. In brief, 769-P and Caki-1 cells were seeded at a density of 5 × 10^4 cells per well in 6-well plates and incubated for 24 hours. At 50-60% confluence, cells were transduced with either sh-STAC3 or NC using 8 μg/ml polybrene (JiKai Gene Technologies), in accordance with the manufacturer's protocol. After 72 hours of transduction, cells were cultured and selected with 2 μg/μl puromycin to isolate stably transduced cells. The silencing efficiency of STAC3 was then verified by Western blot analysis.

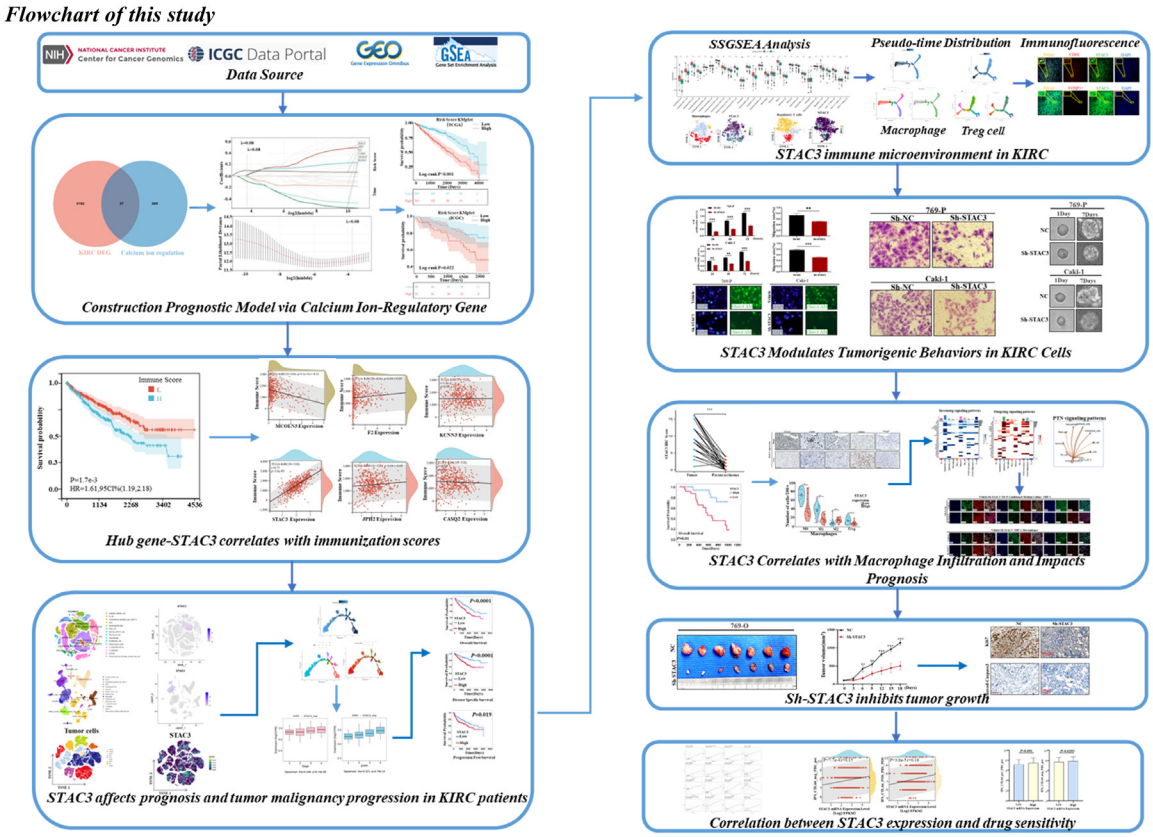


**Figure 1.** Flowchart of this study.

*Western blot*

Cell lysis was performed using RIPA lysis and extraction buffer, enhanced with a cocktail of phosphatase and protease inhibitors (Seven, China). Proteins were then separated by SDS-PAGE and transferred to membranes via semi-dry blotting, adhering to established protocols. These membranes were incubated at 4°C overnight with primary monoclonal antibodies targeting STAC3 (Cat No. 20392-1-AP; 1:5000, Proteintech, China), STAT3 (Cat No. 10253-2-AP; 1:2000, Proteintech, China), Phospho-Stat3 (#9145; 1:2000, Cell Signaling Technology, USA), Jak2 (#3230; 1:2000, Cell Signaling Technology, USA), Phospho-Jak2 (#8082; 1:1000, Cell Signaling Technology, USA), and Beta Actin (Cat No. 81115-1-RR; 1:5000, Proteintech, China). Subsequent to the primary antibody incubation, membranes were treated with horseradish peroxidase-conjugated secondary antibodies (anti-mouse and anti-rabbit, both 1:5000 in TBST) for chemiluminescent detection. Beta Actin served as the loading control. Quantitative analysis of the protein bands was conducted using ImageJ software (version 1.48v; National Institutes of Health, Bethesda, MD, USA).

*MTT (3-[4,5-dimethylthiazol-2-yl]-2,5-diphenyl-tetrazolium bromide) assay*

Cells, upon reaching their logarithmic growth phase, were plated at 2,000 cells per well in a 96-well plate. Cell viability was assessed at 24, 48, and 72 hours post-treatment with Sh-STAC3 and vector control using the MTT assay. For this, 15 µl of MTT solution (5 mg/ml, Sigma-Aldrich, MO, USA) was introduced to each well and incubated for 4 hours. After incubation, the supernatant was discarded, and 100 µl of DMSO (Sigma-Aldrich, MO, USA) was added to dissolve the formazan crystals. Absorbance was measured at 570 nm, with a reference wavelength of 630 nm, using a microplate reader. All procedures were replicated three times to ensure consistency.

*Wound healing assay*

Stable knockdown of STAC3 was achieved in KIRC cells (769-P and Caki-1) through transfec-

tion with STAC3 expression vectors or control vectors. The transfected cells were seeded into 6-well plates and cultured until 80% confluence. A scratch was made on the monolayer using a 200 μl pipette tip. The scratched area was then carefully washed with PBS to remove any detached cells. Cells were subsequently cultured in DMEM base medium. Immediately after scratch creation, the wounded area was observed under a microscope and photographed. Additional photographs were taken after 24 and 48 hours of culture. All experimental data were derived from at least three independent replicate experiments to ensure reliability and reproducibility of the data.

*Cell Invasion assay*

For the cell invasion assay, transwell chambers precoated with Matrigel® (Corning 354480) were utilized. A cell suspension of 1.5 × 10^5 cells in 200 μl serum-free medium was seeded into the upper chamber. The lower chamber was filled with 600 μl of culture medium supplemented with 10% fetal bovine serum to serve as a chemoattractant. After a 36-hour incubation, the cells were fixed in 100% methanol and stained with a 10% Giemsa solution (Sigma-Aldrich, Cat# 12-0440). Cell counts were performed using ImageJ software (National Institute of Health, USA).

*3-D cell culture*

Each well of a 48-well plate was uniformly coated with 150 μl of Matrigel and placed on ice. Following this, the plates were centrifuged at 4°C and 300 × g for 5 minutes. They were then incubated in a cell culture incubator for 30 minutes to solidify the Matrigel. Single cell suspensions were prepared in a medium containing 10% Matrigel, with a density of 500 cells per 200 μl, and seeded onto the Matrigel-coated wells. Cells were allowed to adhere to the Matrigel for 3 hours. After this period, the medium was gently aspirated and replaced with fresh medium containing 10% Matrigel. An additional hour of incubation was followed by the addition of the appropriate medium. The medium was refreshed every two days with 10% Matrigel to maintain the culture. Photographs of the 48-well plates were taken every three days to monitor spheroid size in each well. To ensure reproducibility, all experiments were conducted in triplicate under each set of conditions.

*Subcutaneous tumor models*

Stably transfected 769-P cells (5 × 10^6 cells in 0.1 mL PBS), either with an empty vector (control) or Sh-STAC3, were subcutaneously injected into the left shoulders of nude mice. The mice were randomly allocated into two groups (n=7 per group): a control group and a Sh-STAC3 group. Tumor volumes (mm^3) were calculated using the formula: length × depth^2 × π/6. Tumor size was measured with calipers every three days once the volume reached 100 mm^3 to track tumor growth. After three weeks, the mice were euthanized, and the tumors were excised, weighed, and fixed in 10% neutral buffered formalin for subsequent analyses.

*Immunohistochemistry (IHC)*

IHC staining on 4 μm thick FFPE tissue sections utilized specific antibodies against STAC3 (Cat No. 20392-1-AP; 1:400, Proteintech, China), CD68 (Cat No. 66231-2-Ig; 1:1000, Proteintech, China), CD80 (Cat No. 66406-1-Ig; 1:500, Proteintech, China), CD163 (Cat No. 68218-1-Ig; 1:2500, Proteintech, China), FOXP3 (ab20034; 1:250, Abcam, Cambridge, UK), Ki67 (Cat No. 27309-1-AP; 1:2000, Proteintech, China), and Cleaved Caspase-3 (#9661; 1:2000, CST, USA). Deparaffinization of sections was conducted in xylene, followed by rehydration in a descending ethanol series. Antigen retrieval involved heating the sections in Citric Acid Based Antigen Unmasking Solution (Vector Laboratories, Burlingame, CA) for 6 minutes in a microwave pressure cooker, then cooling for 30 minutes. Blocking was achieved using a solution containing 5% normal goat serum, and the sections were incubated with primary antibodies at 4°C overnight. Following a PBST rinse, the sections were incubated with secondary antibodies. DAB tablets (Wako Chemicals, Richmond, VA) were employed for color development as per the manufacturer's guidelines. The sections were counterstained with hematoxylin, dehydrated, and mounted in neutral resin. STAC3 expression was quantitatively evaluated by three blinded pathologists using a semiquantitative scoring system, considering both staining distribution and intensity, with the final score being the multiplication of these two parameters.

*Immunofluorescence assay*

The cells were fixed with 4% paraformaldehyde for 15 minutes at room temperature (Tissue paraffin sections, then closed after gradient dehydration and completion of antigen repair). After blocking with goat serum in PBS for 30 min, cells/tissues were stained with primary antibody (STAC3 (Cat No. 20392-1-AP; 1:500, Proteintech, China), CD68 (Cat No. 66231-2-Ig; 1:3000, Proteintech, China), CD80 (Cat No. 66406-1-Ig; 1:200, Proteintech, China), CD163 (Cat No. 68218-1-Ig; 1:600, Proteintech, China), FOXP3 (ab20034; 1:150, Abcam, Cambridge, UK)) at 4°C overnight and then washed three times with PBST. The cells were incubated with the secondary antibody at a dilution of 1: 50 for 1 hour at room temperature in the dark. Secondary antibodies were purchased from ABCLONAL (FITC Goat Anti-Rabbit IgG, Cat No. AS011, 1:75; TRITC Goat Anti-Mouse IgG, Cat No. AS026, 1:75). Finally, the cells/tissues were washed three times with PBST and counterstained with DAPI (Cat No. P0131, beyotime, China). Confocal imaging was conducted using a Nikon C2+ microscope system with standard filters and NIS-Elements software.

*Intracellular calcium ion concentration was assessed with Fluo-4 AM*

Measurement of Intracellular $Ca^{2+}$ levels were determined using a Fluo-4 AM calcium assay kit (Beyotime, Jiangsu, China) according to the manufacturer's instruction. Briefly, the cells were seeded in 6-well black plates with a density of $5 \times 10^4$/ml with 6 parallel wells in each group. Cells were stained with 5 μM Fluo-4 AM at 37°C in the dark for 30 mins. Then cells were washed with PBS three times, and the level of fluorescence was determined by Flexstation®2 fluorescence plate reader at 488/516 nm and by microscopy (Leica).

*Co-culture of tumor cells with macrophages*

We collected 769-P cells (Vehicle or Sh-STAC3) in conditioned medium for the culture of human macrophages THP-1. Briefly, we first induced THP-1 cells to differentiate into macrophages using the phorbol 12-myristate 13-acetate (PMA). After the cells adhered, we replaced the macrophage medium with a mixed medium (tumor cell conditioned medium: DMEM-H complete medium, 1:1) for co-culturing for 72 h. Macrophages were subjected to immunofluorescence staining.

*Bioinformatics analysis*

In this study, bioinformatics approaches were utilized to analyze KIRC data. A cohort of 531 tumor and 72 normal tissue samples, along with clinical information, was obtained from the TCGA database (https://portal.gdc.cancer.gov/) to investigate differential gene expression and its prognostic implications. Additionally, clinical and transcriptome data of 91 KIRC samples were sourced from the ICGC database (https://dcc.icgc.org) for further analysis. From the GSEA database (https://www.gsea-msigdb.org/), 237 genes associated with calcium ion regulation were extracted.

Using the R package glmnet, a clinical predictive model incorporating six genes was constructed by integrating KIRC patient survival time, survival status, and calcium ion-regulating gene expression data, employing the lasso-cox regression method with 10-fold cross-validation. The optimal model, with a Lambda value of 0.0750554516401776, included the following genes: RiskScore = 0.015317484123409STAC3 + 0.0211261199780643JPH2 - 0.0951982243382876KCNN3 - 0.00324917828076427CASQ2+0.0957639132957437F2 - 0.0183582615073728MCOLN3.

The ESTIMATE algorithm was applied to predict cell infiltration levels in tumor tissues, based on a preselected matrix/immune-related gene set and gene expression data, yielding stroma and immune scores and an overall estimate score for KIRC patients. The impact of these scores on KIRC prognosis was analyzed.

Differences in immune cell infiltration between normal and cancer tissues and the influence of STAC3 expression on this infiltration were investigated using the GSVA R package and Spearman analysis, employing the Single-sample gene set enrichment analysis (ssGSEA) method.

The role of STAC3 across various cancers was explored using the LinkedOmicsKB database (https://kb.linkedomics.org). Additionally, the expression of STAC3 at the single-cell level in tumor tissues was further analyzed using the TISCH database (TISCH (comp-genomics.org)).

The methodology for analyzing drug sensitivity in relation to STAC3 expression involved Spearman correlation analysis. RNA expression data and pharmacological profiles were downloaded from the CellMiner database (https://discover.nci.nih.gov/cellminer/home.do).

Moreover, ROC and time-dependent ROC (tROC) curve analyses were conducted using the pROC and survival-ROC packages, with data visualization performed using the R package ggplot2.

The STAC3 high and low expression groups were further analyzed for differentially expressed genes through the TCGA database. The differentially expressed genes were further mapped with volcano maps and subjected to Kegg and GO (BP, CC, MF) enrichment analysis, and visualized using ggplot2.

*Preprocessing of single-cell RNA sequencing data*

Using the "Seurat" package (version 4.4.0), we constructed Seurat objects based on single-cell transcriptomic expression matrices for both global and specific cell types. Cells expressing between 200 and 2000 RNA features were selected. Additionally, a threshold of 5% mitochondrial RNA was set for normalizing single-cell RNA sequencing data. The "harmony" algorithm was employed to eliminate batch effects between samples (Supplementary Figure 1). Furthermore, we used the "ScaleData" and "RunPCA" functions to determine the number of principal components (PCs) based on the Seurat objects, adjusting the number of PCs to 15 to form cell clusters, which were then visualized using UMAP plots. For annotating the cell clusters, unsupervised clustering was performed using the "FindClusters" and "FindNeighbors" functions. The clustering results exhibited optimal clarity when the resolution was set to 0.3. Finally, automated cell type annotation for each cluster was conducted using the "SingleR" package (version 1.4.1) and manual annotation (cell marker2.0) based on the marker genes of each cluster.

*Cell-cell communication analysis*

The CellChat package serves as an effective analytical tool for exploring intercellular communication and interactions. In this study, we utilized CellChat to analyze key biological interactions among cells in KIRC, calculating the probability and significance of these interactions. To visually represent the relationships and importance of these interactions, we employed circle and bubble plots for visualization.

*Pseudo-time trajectory*

In this study, we utilized the Monocle 2 algorithm (version 2.22.0) to extract expression matrices and relevant information from processed Seurat objects, thereby creating a Monocle object. We conducted pseudotime analysis on specific subsets of cells obtained through subset functionality, including KIRC cells, T cells, and macrophages. The analysis involved initially sorting cells and constructing their developmental trajectories using the order Cells function, followed by dimensionality reduction using the DDRTree algorithm. Finally, we utilized the plot_genes_in_pseudotime function to plot gene expression over pseudotime, and separately generated violin plots, trajectory point plots, and trend plots using plot_genes_jitter, plot_cell_trajectory, and plot_genes_in_pseudotime, respectively. Lastly, we performed gene clustering analysis using the plot_pseudotime_heatmap function and visualized pseudotime differential genes via heatmap. Additionally, single-cell regulatory network interference and clustering (SCENIC, version 1.2.4) was employed on all single cells to unveil the regulatory relationships between transcription factors (TFs) and target genes. The "limma" package was utilized to calculate significantly distinctly expressed regulators, with a statistical significance level set at $P < 0.05$.

*Statistical analysis*

Data were reported as mean ± standard deviation (SD). Statistical analyses were carried out with SPSS software, version 26.0 (SPSS Inc., IL, USA). Group differences were assessed using one-way ANOVA, complemented by Dunnett's t-test for post hoc comparisons. A *P*-value below 0.05 was deemed to indicate statistical significance.

## Results

*The prognostic impact of $Ca^{2+}$ regulatory genes in KIRC'*

The notoriety of KIRC stems from its poor prognosis, attributed to diagnostic and therapeutic challenges, high chemoresistance, and subop-

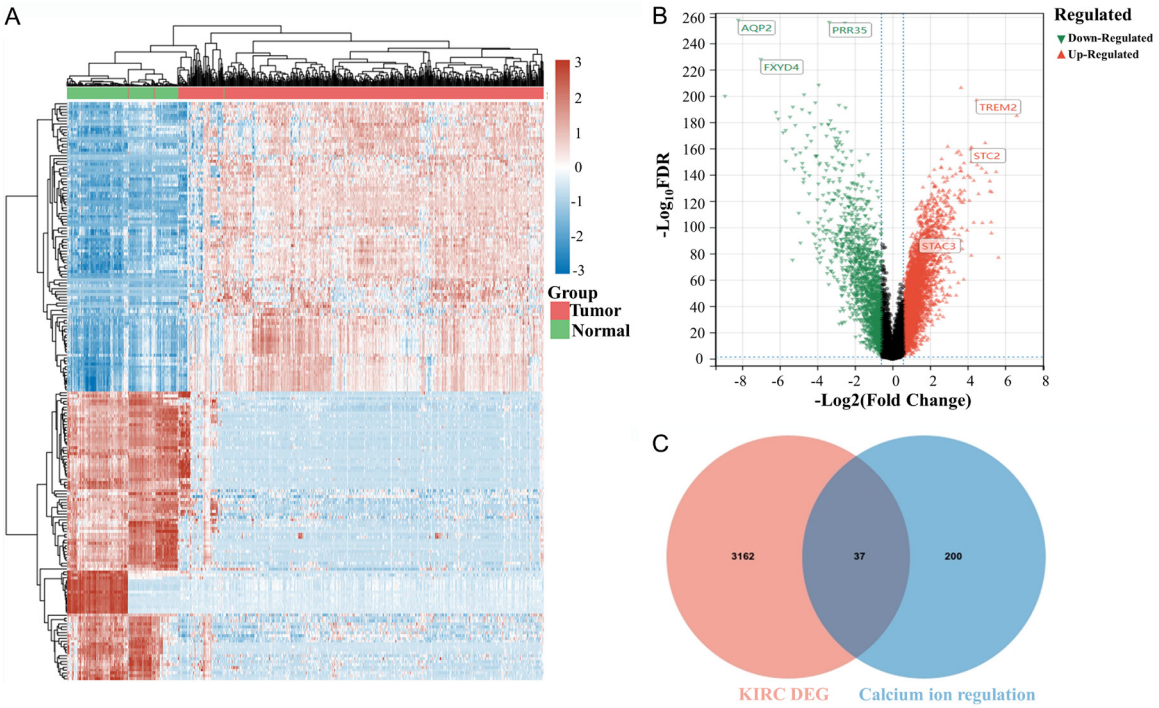


**Figure 2.** Screening of differentially expressed genes in KIRC associated with calcium ion regulation. A: Heatmap of gene expression differences in KIRC compared to normal tissue; B: Genes up-regulated and down-regulated in KIRC (Volcano plot, Red: up-regulated; Blue: down-regulated); C: Genes related to calcium ion regulation in KIRC.

timal immunotherapy outcomes [32]. This underscores the necessity for comprehensive investigations into KIRC's etiology. The impact of $Ca^{2+}$ regulatory genes on KIRC's prognosis and their role in oncogenic pathways has not been sufficiently examined [11].

Our examination of KIRC samples, using the TCGA database, identified 3,119 differentially expressed genes (DEGs), with 2,228 upregulated and 891 downregulated. These DEGs are depicted in heatmaps and volcano plots (**Figure 2A**, **2B**). Cross-referencing GSEA database findings, we located 237 $Ca^{2+}$ regulation genes, which, when cross-matched with KIRC DEGs, resulted in 37 related DEGs (**Figure 2C**). Further scrutiny disclosed 21 genes with prognostic influence on KIRC (**Figure 3A**).

Employing lasso-cox regression analysis with survival, status, and gene expression data, we constructed an optimal model comprising six pivotal genes (F2, STAC3, CASQ2, JPH2, MCOLN3, KCNN3) (**Figure 3B**). A risk score analysis, incorporating patient follow-up and hub gene expression, indicated a significant survival reduction correlating with higher risk scores. CASQ2, MCOLN3, and KCNN3 were identified as protective, with their decreased expression linked to elevated risk scores, while STAC3, JPH2, and F2 emerged as risk-enhancing factors due to their increased expression (**Figure 3C**).

Further validation using TCGA and ICGC datasets demonstrated that patients with elevated risk scores had a significantly poorer prognosis (**Figure 3D**). ROC curve analysis verified the risk score's effectiveness in prognostic prediction, with substantial AUC values in both datasets (**Figure 3E**). Multivariate COX analysis confirmed the risk score's status as an independent prognostic indicator (**Figure 3F**).

*Abnormal immune regulation in KIRC, with STAC3 implicated in cancer immunity*

Recent investigations have elucidated the pivotal role of various immune cells in shaping the prognosis of KIRC, as evidenced by studies [15, 24]. In an endeavor to discern the impact of tumor immunity on the prognosis of KIRC patients, we employed the ESTIMATE algorithm to calculate the Immune Scores of patients and examined their influence on the prognosis of KIRC. The findings suggest that elevated

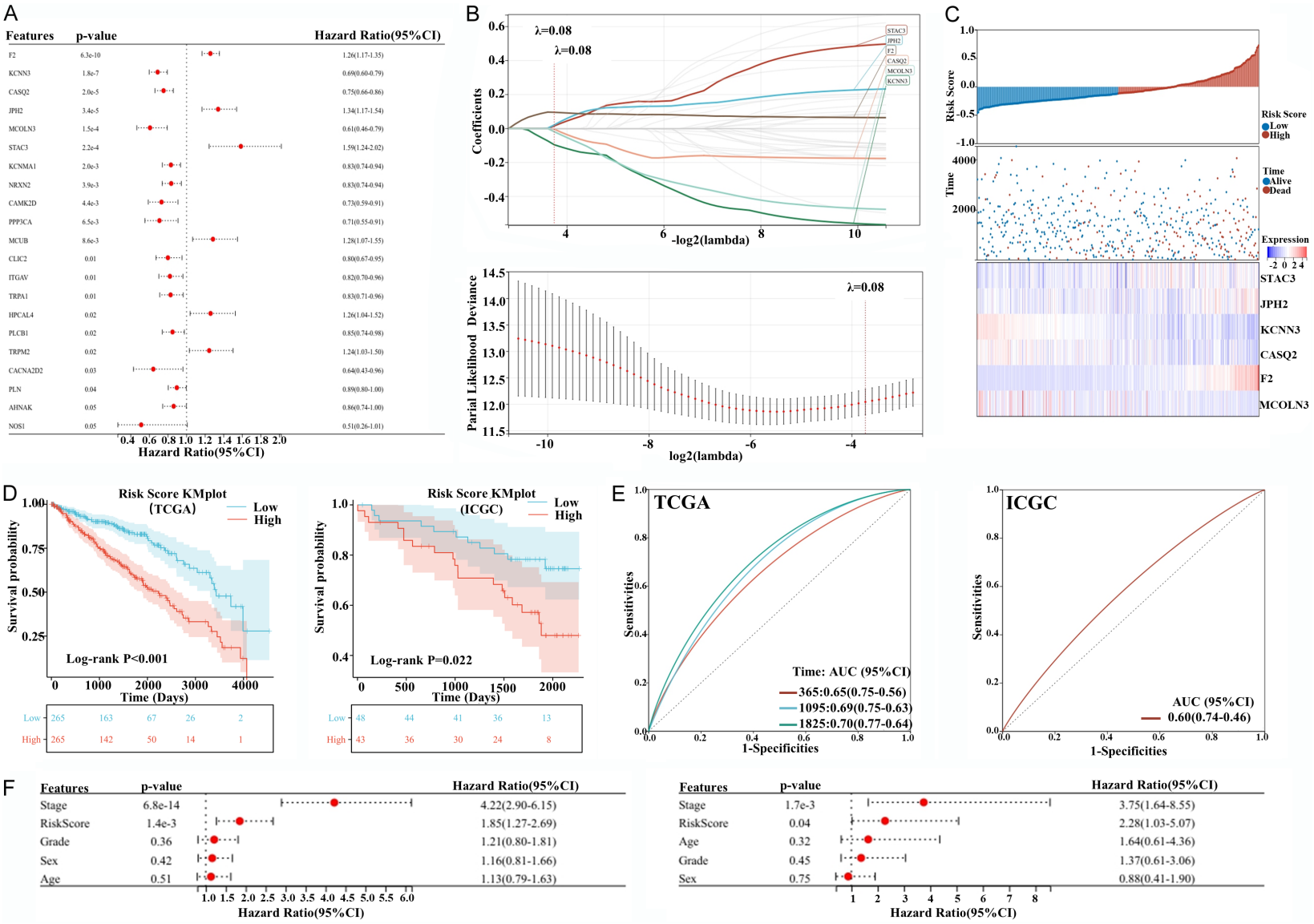


**Figure 3.** Development of a prognostic model via calcium ion-regulatory gene expression. A: Prognostic impact of gene expression modulated by calcium ion regulation in KIRC patients; B: Clinical prognostic model formulation using lasso-Cox regression analysis; C: Heatmap illustrating the correlation between RiskScore and hub gene expression; D: Kaplan-Meier plots demonstrating Risk Score's prognostic significance (Training set: TCGA; Validation set: ICGC); E: ROC curves assessing Risk Score's predictive accuracy for patient outcomes (Training set: TCGA; Validation set: ICGC); F: Multivariate Cox regression analysis establishing Risk Score as an independent prognostic indicator (Training set: TCGA; Validation set: ICGC).

Immune Scores in KIRC patients are correlated with adverse prognostic outcomes (**Figure 4A**). Subsequent analysis through Single Sample Gene Set Enrichment Analysis (ssGSEA) delineated a stark disparity in immune cell infiltration between KIRC tumors and normal tissues, categorizing the tumor as immunologically 'hot' - a feature less commonly seen in the typical tumor immune landscape (**Figure 4B**). Moreover, an assessment via monocle2 of the incoming signals in different cells within normal and tumor tissues revealed an aberrantly high activity of incoming signals in various immune cells within tumor tissues, including CSF in macrophages, IL16, and MK cell pathways, as well as CD137, MK, SPP1 signaling pathways in regulatory T cells (Tregs). These observations indicate that certain cells in tumor tissues may become abnormally activated upon stimulation by some incoming signals (**Figure 4C**). Further evaluation of the outgoing signals in different cells within normal and KIRC tissues mirrored the previous findings, showcasing an abnormal activity of various outgoing signals in cells including macrophages, Tregs, CD8+/CD3+ T cells, and KIRC tumor cells (**Figure 4D**). Additionally, our analysis of intercellular communication within normal and tumor tissues demonstrated that communication among cells in tumor tissues was notably active, particularly between tumor cells and macrophages, T cells, and memory CD4+ T cells (**Figure 4E**, **4F**). Detailed examination of specific immune cell groups identified several, including CD4+ T cells, NKT cells, monocytes, M1 macrophages, and CD8+ T cells, as risk factors for negative outcomes (Hazard Ratio [95% CI] > 1), and Myocytes cells as a protective factor for positive outcomes (Hazard Ratio [95% CI] < 1) (Supplementary Figure 2). These insights might be associated with KIRC-induced angiogenesis within the tumor's immune architecture, diminished TLS density, and increased recruitment of immature dendritic cells, which collectively facilitate the proliferation of Tregs [16, 32]. Further correlation analyses between hub genes (F2, STAC3, CASQ2, JPH2, MCOLN3, KCNN3) and prognostic scores (Stromal, ESTIMATE, and Immune Scores) highlighted STAC3's significant positive correlation, underlining its critical role in modulating the immune microenvironment of KIRC and its prognosis (**Figure 4G**, Supplementary Figure 3). These results illuminate the disparities in immune cell infiltration within KIRC tissues and suggest that the unusually active communication between tumor tissues and various immune cells, including macrophages, may be a key determinant of poor prognosis in KIRC patients, with STAC3 potentially playing a crucial role.

*STAC3's role in the differentiation and malignancy of KIRC tumors*

To further explore the role of STAC3 in cancer progression, this study utilized the LinkedOmicsKB database to analyze the expression of STAC3 across various cancer types and its impact. The analysis revealed a significant correlation between STAC3 expression and macrophage, tumor immune scoring, and the activation of the IL6/JAK/STAT3 signaling pathway (Supplementary Figure 4A). Further investigation through single-cell sequencing analysis and the TISCH database on KIRC tissues identified a predominant enrichment of STAC3 in the monocyte-macrophage lineage and memory CD4+ T cells (**Figure 5A**, Supplementary Figure 4B). This finding supports our hypothesis that the unusually active communication between KIRC tumor cells and macrophages, as well as memory CD4+ T cells, may be associated with high STAC3 expression. We analyzed KIRC tumor cells alone which showed that STAC3 was expressed on tumor cells. Pseudotime analysis reveals the differentiation trajectory of KIRC tumor cell subpopulations, where cells in similar states are grouped together, and distinct states are separated by branching points. After further dimensionality reduction and clustering, 6 clusters are identified within KIRC tumor cell subpopulations. Characteristic markers for clusters 2 and 5, such as CPE and SRGN, are associated with tumor proliferation-related genes. Therefore, clusters 0 are determined as the starting point of the pseudotime trajectory, while clusters 2 and 5 serve as endpoints. Simultaneously, pseudotime analysis subdivides the developmental process of KIRC tumor subpopulations into 11 stages (**Figure 5B**). We observe the highest expression of STAC3 in state 7, and the expression pattern of STAC3 in pseudotime correlates significantly with the malignant degree of the tumor, as reflected by the expression of marker genes of KIRC cells in state 7 (**Figure 5C**). Based on the malignancy degree of KIRC, we divided it into seven clusters, with the highest STAC3 expression found

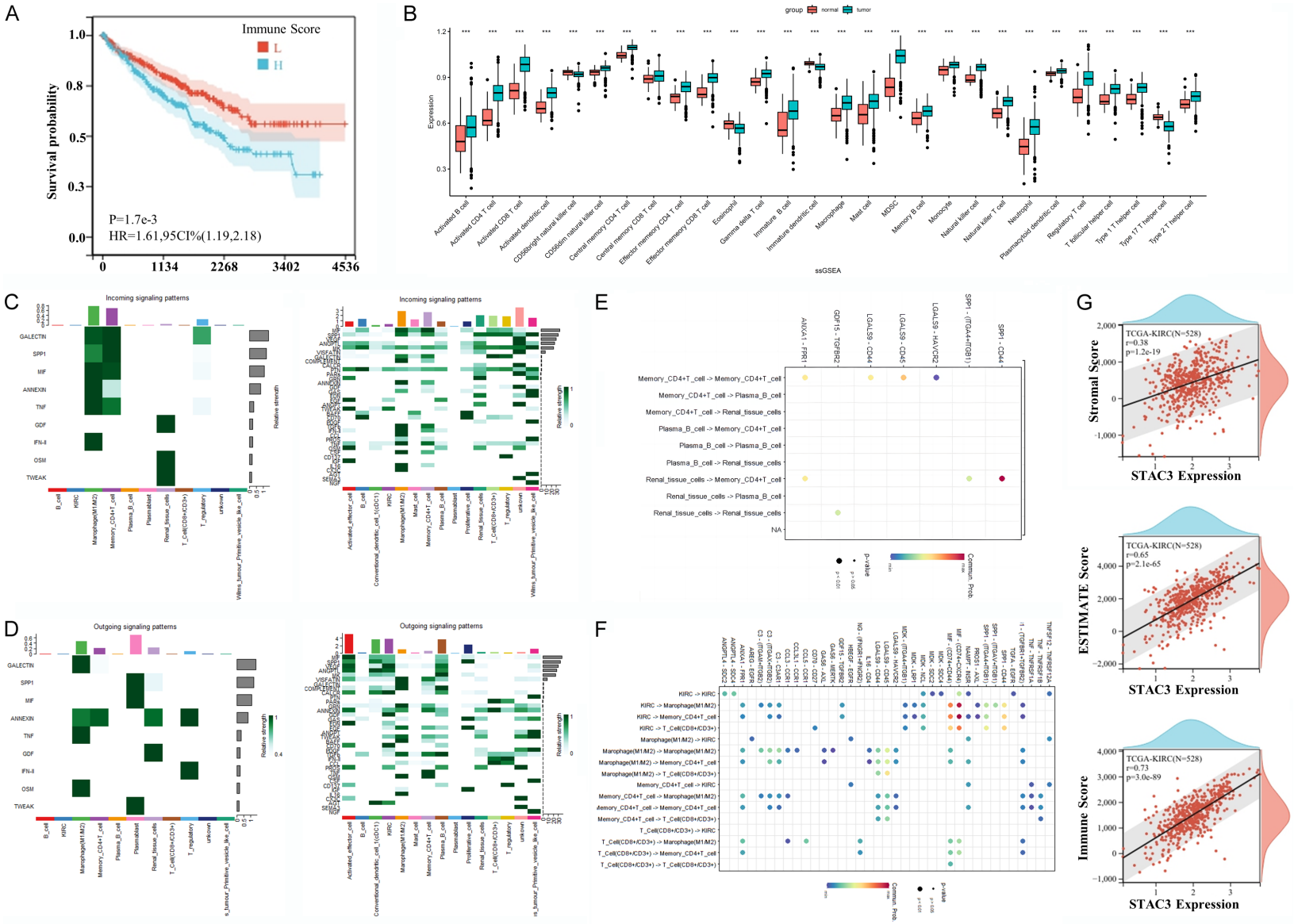


**Figure 4.** Abnormal immune regulation in KIRC, with STAC3 implicated in cancer immunity. A: High immune score associated with poor prognosis in patients with high KIRC expression; B: Differential infiltration of various immune cells in KIRC tumor tissues compared to normal tissue; C: Abnormal activation of multiple incoming signal patterns in immune cells within KIRC tumors relative to normal tissue; D: Increased activity of multiple outgoing signal patterns in immune cells within KIRC tumors compared to normal tissue; E: Communication networks between immune cells in normal tissue; F: Enhanced intercellular communication within KIRC tumors; G: Correlation analysis of STAC3 with stromal score, ESTIMATE score, and immune score in tumor tissue. *, P < 0.05; **, P < 0.01; ***, P < 0.001; ****, P < 0.0001.

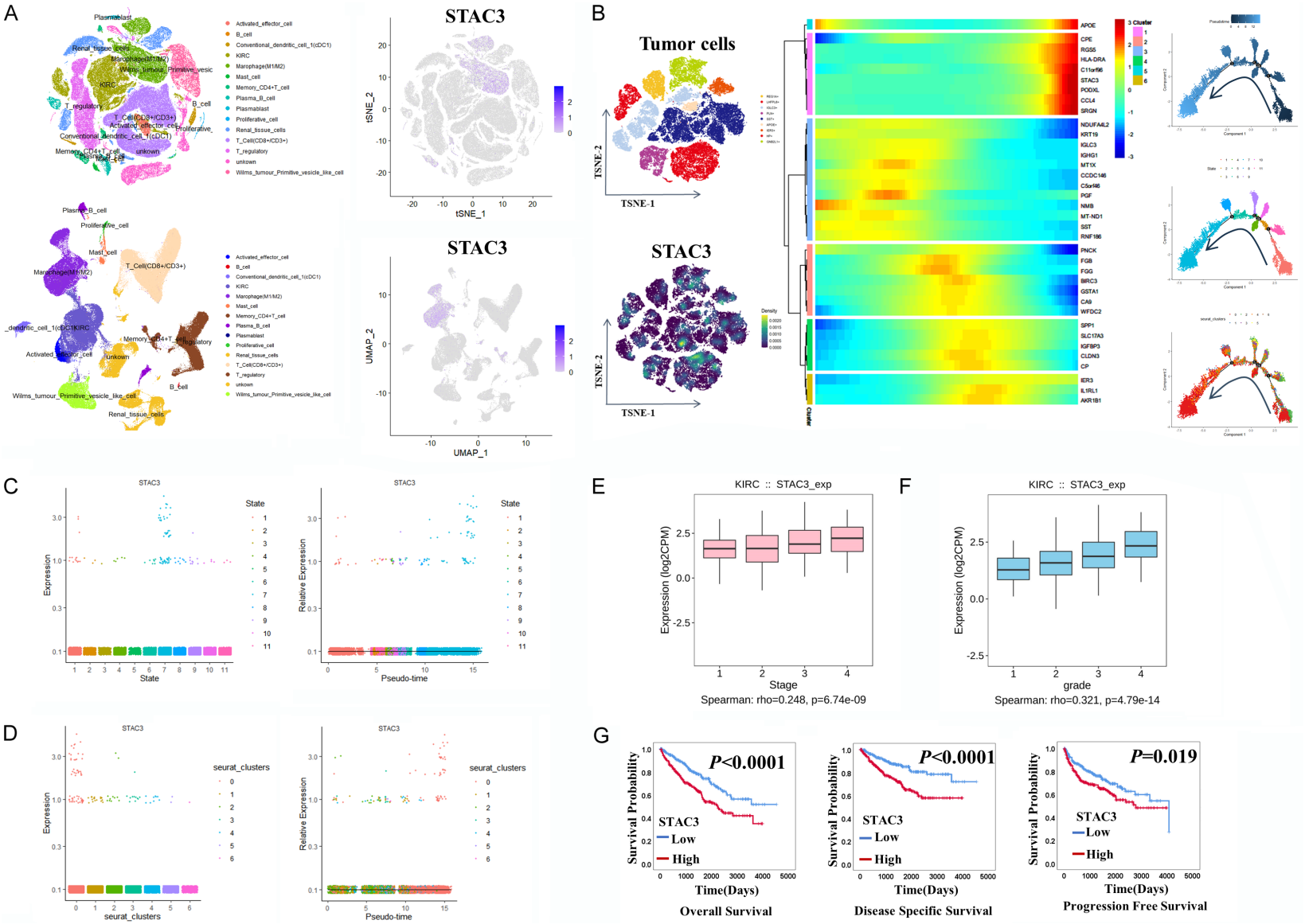


**Figure 5.** STAC3's role in the differentiation and malignancy of KIRC tumors. A: Single-cell sequencing reveals an enrichment of STAC3 in tumor-associated macrophages and CD4+ T cell subsets within KIRC tissues; B: Expression of STAC3 in KIRC tumor cells and pseudo-time distribution of the different KIRC cell subtypes,

heatmap showing the change of potential feature genes in pseudo-time developmental trajectories; C: Variations in STAC3 expression are observed across different stages of KIRC differentiation; D: Distinct KIRC subgroups exhibit differential STAC3 expression patterns; E: Positive correlation between STAC3 expression and tumor staging in KIRC tissues; F: Positive correlation between STAC3 expression and tumor grading in KIRC tissues; G: STAC3 expression impacts Overall Survival, Disease-Specific Survival, and Progression-Free Survival in KIRC patients.

in cluster 0. Pseudotime analysis indicated that cluster 0 KIRC had a higher malignancy degree, being in the later stages of tumor development, further confirming that high STAC3 expression is associated with an increase in tumor malignancy degree, and as the tumor progresses to a more malignant phenotype, the expression level of STAC3 also increases (**Figure 5D**). In the later stages of KIRC tumors, STAC3 expression is higher, showing a positive correlation with tumor staging (**Figure 5E**). Additionally, STAC3 expression is higher in KIRC tissues with a higher Grade classification (**Figure 5F**). Subsequent research has clarified the impact of STAC3 on the prognosis of KIRC patients, finding that a higher level of STAC3 expression is inversely related to overall survival, disease-specific survival, and progression-free survival rates (**Figure 5G**). In summary, our analysis reveals a close relationship between STAC3 and tumor immunity, as well as the significant impact of STAC3 on the malignant differentiation and poor prognosis of KIRC tumors, suggesting STAC3 as a potential therapeutic target for improving cancer prognosis.

*STAC3 modulates tumor immune infiltration and differentiation of macrophages and regulatory T cells*

SSGSEA analyses substantiate marked disparities in immune cell infiltration based on the differential expression of SATC3, observing that tissues with elevated STAC3 expression are frequently characterized by an enhanced presence of macrophages, Tregs, CD8+ T cells, and CD4+ T cells (**Figure 6A**). The critical function of macrophages and Tregs within the tumor microenvironment - specifically within the tumor core, invasive edges, and stroma, and their prognostic relevance across a multitude of cancers - highlights the necessity to investigate the mechanisms through which STAC3 influences macrophage functionality and infiltration.

Single-cell sequencing showed that STAC3 was expressed in macrophages and Tregs (**Figure 6B-D**, Supplementary Figure 5). Pseudotime analysis, utilized to delineate the various developmental stages of macrophages, demonstrates that cells exhibiting similar states congregate, with divergent states delineated by branching points, notably positioning macrophages in clusters 1 and 6 at the terminal of the pseudotime trajectory. A set of 36 potential characteristic genes pertinent to macrophages was identified within the human transcriptional gene pool, and the expression variations of these genes were monitored across different macrophage subpopulations, revealing a significant upregulation of STAC3 in cluster 1 cells (**Figure 6E**). Correspondingly, pseudotime analysis delineated varied Tregs developmental stages with differential STAC3 expressions, locating Tregs in cluster 1 at the pseudotime trajectory's terminus. From the human transcriptional gene repository, 36 potential Tregs-related characteristic genes were discerned, and the expression dynamics of these genes across Tregs subgroups were tracked, uncovering a pronounced increase in STAC3 expression within cluster 1 cells (**Figure 6F**). Collectively, these observations affirm the integral association between STAC3 expression and the differentiation of macrophages and Tregs, underscoring the significance of identifying cell subpopulations based on STAC3 expression in macrophages and Tregs for a comprehensive analysis of their contribution to tumor immune infiltration. Immunofluorescence staining further confirmed that STAC3 is expressed not only in KIRC tumor cells but also in macrophages and Tregs, with overlapping expression locations with CD68 (a macrophage marker) and Foxp3 (a Treg marker) (**Figure 6G**).

*STAC3 modulates functional dynamics of KIRC cells*

To further elucidate the role of STAC3 in tumorigenic activities, we investigated its effects on the proliferation, invasion, and migration of KIRC cells, specifically in the 769-P and Caki-1 cell lines, where the STAC3 gene was knocked down (**Figure 7A**, **7B**). MTT assays demonstrated that knockdown of STAC3 significantly inhibited cell proliferation at 24, 48 and 72 hours post-treatment (**Figure 7C**). Staining of intracel-

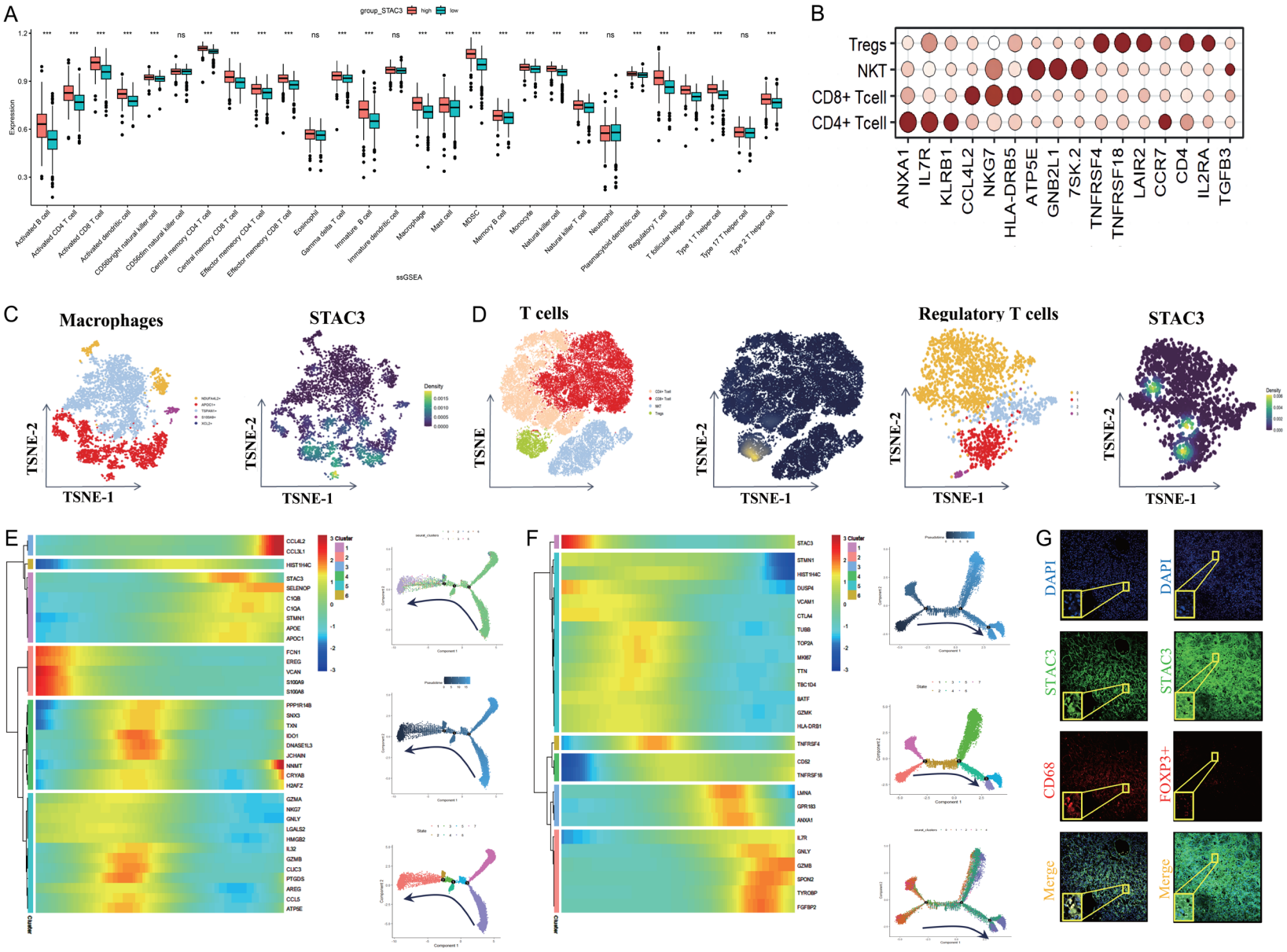
A
group_STAC3 high low
Expression
ssGSEA
Activated B cell
Activated CD4 T cell
Activated CD8 T cell
Activated dendritic cell
CD56bright natural killer cell
CD56dim natural killer cell
Central memory CD4 T cell
Central memory CD8 T cell
Effector memory CD4 T cell
Effector memory CD8 T cell
Eosinophil
Gamma delta T cell
Immature B cell
Immature dendritic cell
Macrophage
Mast cell
MDSC
Memory B cell
Monocyte
Natural killer cell
Natural killer T cell
Neutrophil
Plasmacytoid dendritic cell
Regulatory T cell
T follicular helper cell
Type 1 T helper cell
Type 17 T helper cell
Type 2 T helper cell
B
Tregs
NKT
CD8+ Tcell
CD4+ Tcell
ANXA1
IL7R
KLRB1
CCL4L2
NKG7
HLA-DRB5
ATP5E
GNB2L1
7SK.2
TNFRSF4
TNFRSF18
LAIR2
CCR7
CD4
IL2RA
TGFB3
C
Macrophages
STAC3
TSNE-1
TSNE-2
D
T cells
Regulatory T cells
STAC3
TSNE
E
F
G
DAPI
STAC3
CD68
FOXP3+
Merge

**Figure 6.** STAC3 modulates tumor immune infiltration and differentiation of macrophages and regulatory T cells. A: Differential immune cell infiltration in KIRC tissues with varying levels of STAC3 expression; B: Marker on the surface of Macrophages and Tregs; C, D: Expression of STAC3 in Macrophages and Tregs cells; E: Pseudo-time distribution of the different macrophage subtypes, heatmap showing the change of potential feature genes in pseudo-time developmental trajectories; F: Pseudo-time distribution of the different Tregs subtypes, heatmap showing the change of potential feature genes in pseudo-time developmental trajectories; G: Immunofluorescence staining shows expression of CD68, STAC3, and FOXP3+ in KIRC tumor tissues.

lular calcium ions by Fluo-4 AM Calcium Ion Probe showed that the concentration of intracellular calcium ions was significantly reduced after STAC3 knocked down (**Figure 7D**). Wound healing assays revealed that the migratory capacity of cells was substantially reduced at 24 and 48 hours following STAC3 silencing (**Figure 7E**, **7F**). Furthermore, Transwell assays indicated that STAC3 knockdown markedly impaired the invasive abilities of the tumor cells (**Figure 7G**, **7H**). Additionally, 3-D cell culture experiments showed that the tumorigenic potential and pseudopodia extensions around the spheroids were notably diminished when STAC3 was suppressed, suggesting its involvement in the cytoskeletal rearrangements associated with cell motility and invasion(**Figure 7I**, **7J**).

To investigate the mechanism of STAC3 on the proliferation and invasion of KIRC tumor cells, we analyzed the differentially expressed genes in the high and low STAC3 expression groups using the TCGA database (Supplementary Figure 6A). We performed KEGG and GO enrichment analysis of these differentially expressed genes, which showed that these differentially expressed genes were mainly associated with tumor immunity and antigen presentation (Supplementary Figure 6B). In addition, some genes are enriched in pathways such as the JAK-STAT signaling pathway and the Toll-like receptor signaling pathway (Supplementary Figure 6C). The JAK-STAT signaling pathway has been extensively studied in renal clear cell carcinoma and is closely related to the proliferation, invasion, and migration of tumor cells, as well as to tumor immune evasion and tumor-associated immune cell infiltration [33]. Our experiments demonstrated that Sh-STAC3 can inhibit the activation of the JAK-STAT signaling pathway in tumor cells, thereby suppressing the expression of downstream cell cycle regulator CyclinD1 and VEGFA, which is related to tumor migration and invasion (Supplementary Figure 6D). In summary, our findings suggest that STAC3 plays a pivotal role in the proliferative, invasive, and migratory behaviors of tumor cells, and targeting STAC3 could potentially enhance the prognosis for KIRC patients.

*Elevated STAC3 expression in KIRC tissues and enhanced macrophage infiltration*

Our investigation into the expression of STAC3 in clinical specimens revealed that STAC3 levels are elevated in tumor tissues compared to normal tissues (**Figure 8A**, **8B**). Correlating with patient clinical data, we observed that patients with higher STAC3 expression have poorer prognoses, aligning with previous findings (**Figure 8C**). High STAC3 expression exhibited increased infiltration of CD68+ M0 macrophages, CD80+ M1 macrophages, and Foxp3+ Tregs, while the infiltration of CD163+ M2 macrophages decreased (**Figure 8D**, **8E**). Correlating this with patient survival information, we found that consistent with bioinformatics analysis, increased infiltration of CD68+ M0 macrophages, CD80+ M1 macrophages, and Foxp3+ Tregs indicated poor prognosis for KIRC patients, whereas increased infiltration of CD163+ M2 macrophages was associated with better prognosis (Supplementary Figure 7A).

To further explore the mechanism by which tumor cells affect macrophage differentiation, we further demonstrated that differential expression of STAC3 affects intercellular signaling through intercellular communication analysis (**Figure 8F**). In outgoing signaling patterns, PTN signaling was abnormally activated in tumor cells with low expression of STAC3, and accordingly, PTN signaling was also abnormally activated in incoming signaling patterns of tumor-associated macrophages. This intercellular communication is completely absent in high STAC3-expressing tumor cells (**Figure 8G**). Several studies have demonstrated that PTN expression is associated with infiltration of CD11b+/CD163+ TAMs [34, 35]. Thus, STAC3 interaction with the PTN signaling pathway may be a key mechanism by which tumor cells influence macrophage infiltration. By receptor-

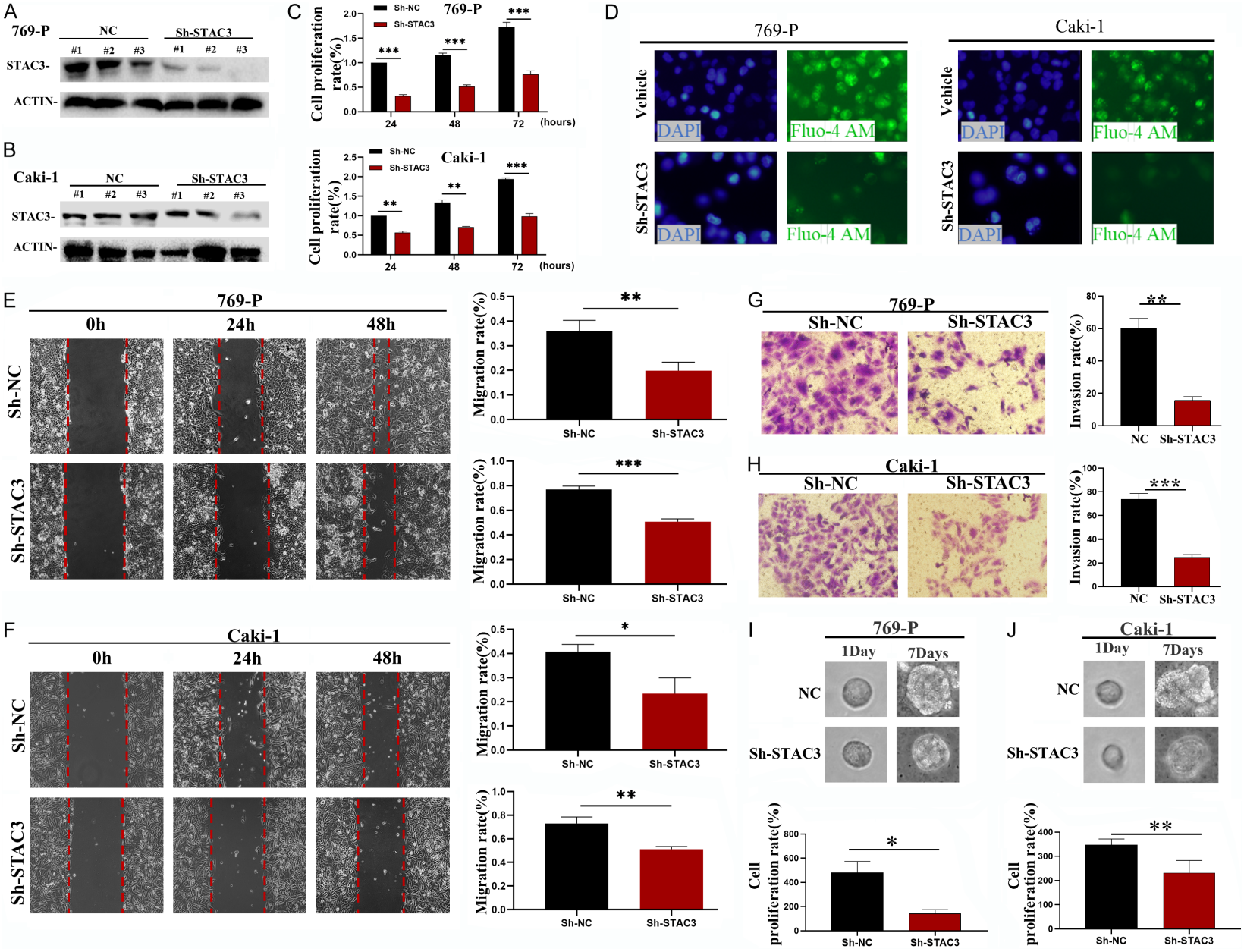
A
769-P
NC
Sh-STAC3
#1 #2 #3 #1 #2 #3
STAC3-
ACTIN-
B
Caki-1
NC
Sh-STAC3
#1 #2 #3 #1 #2 #3
STAC3-
ACTIN-
C
Sh-NC
Sh-STAC3
769-P
Cell proliferation rate(%)
24 48 72 (hours)
Caki-1
D
769-P
Caki-1
Vehicle
Sh-STAC3
DAPI
Fluo-4 AM
E
769-P
0h 24h 48h
Sh-NC
Sh-STAC3
Migration rate(%)
F
Caki-1
G
769-P
Sh-NC
Sh-STAC3
Invasion rate(%)
NC
H
Caki-1
I
769-P
1Day 7Days
J
Caki-1
Cell proliferation rate(%)

**Figure 7.** STAC3 Modulates Tumorigenic Behaviors in KIRC Cells. A, B: STAC3 knockdown in KIRC cells (769-P, Caki-1); C: Sh-STAC3 impairs KIRC cell proliferation over 24, 48, and 72 hours; D: Intracellular calcium ion concentration was down-regulated after Sh-STAC3; E, F: Sh-STAC3 inhibits KIRC cell migration at 24 and 48 hours; G, H: Sh-STAC3 inhibits KIRC cell invasiveness at 36 hours; I, J: Sh-STAC3 decreases KIRC cell proliferation. *, P < 0.05; **, P < 0.01; ***, P < 0.001; ****, P < 0.0001.

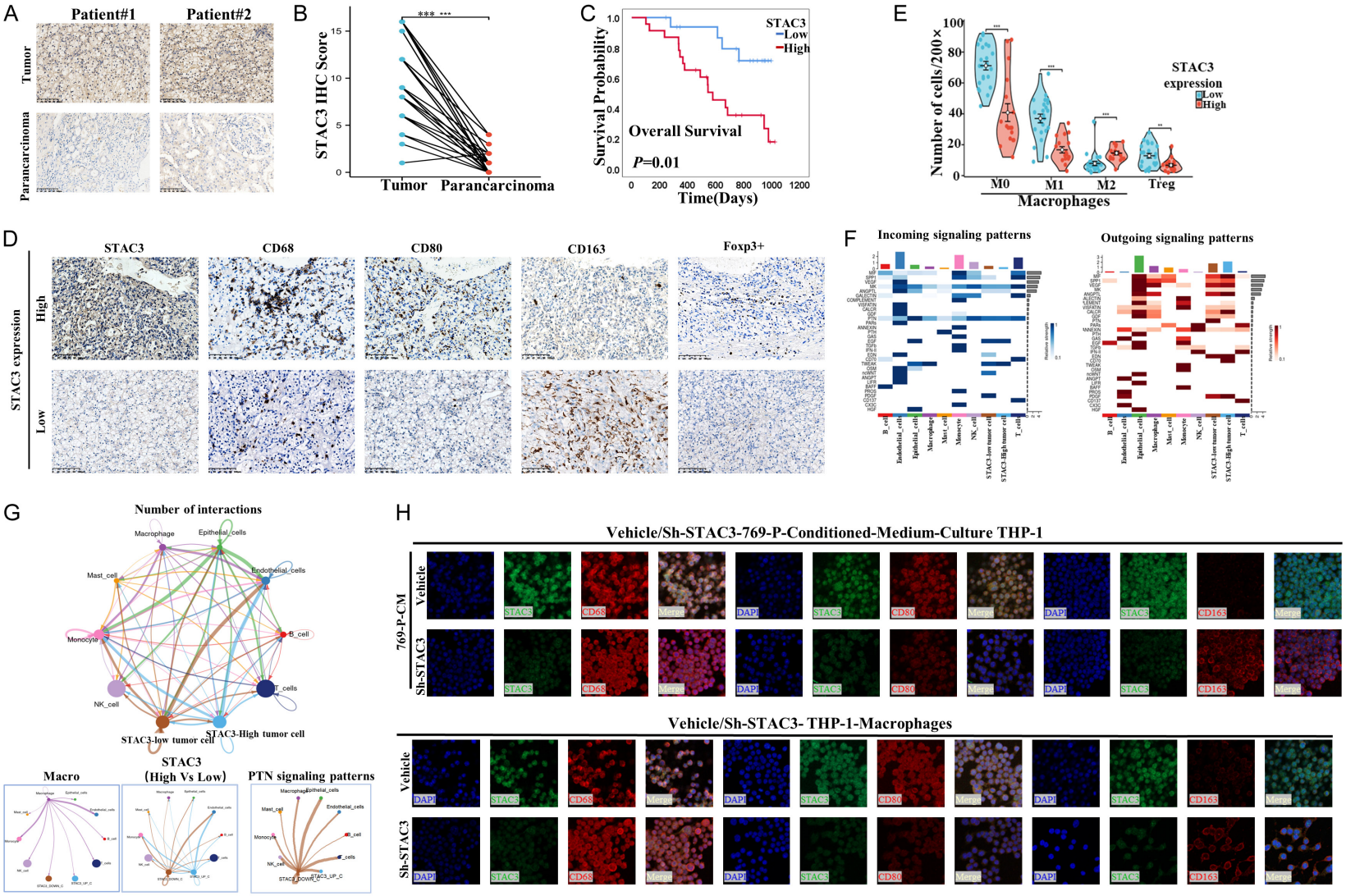

**Figure 8.** STAC3 expression in KIRC tissues correlates with macrophage infiltration and impacts prognosis. A, B: Higher expression of STAC3 in tumor tissues compared to adjacent non-tumor tissues; C: Patients with higher STAC3 expression exhibit worse prognosis in clinical samples; D, E: Differential expression of STAC3 in KIRC tissues affects the expression of CD68, CD80, and CD163; F, G: Expression of incoming and outgoing signaling pathways and intercellular signaling communication in different cells; H: Co-culture of tumor cells-CM with macrophages and expression of sh-STAC3-macrophage associated proteins (STAC3, CD68, CD80, CD163). *, $P < 0.05$; **, $P < 0.01$; ***, $P < 0.001$; ****, $P < 0.0001$.

ligand pair analysis, we found that ANGPTL4-SDC4 was aberrantly activated between low-expressing STAC3 tumor cells and macrophages, whereas this mechanism was not apparent between high-expressing STAC3 tumor cells and macrophages (Supplementary Figure 7B).

To further analyze the impact of STAC3 expression on macrophage infiltration, we cultured the macrophages with conditioned media from 769-P stable cell lines (vehicle and Sh-STAC3). The results showed that macrophages cultured with conditioned media from Sh-STAC3-769-P cells had downregulated expression of STAC3 and CD80, and upregulated expression of CD163. Therefore, the expression of STAC3 in KIRC tumor cells affects macrophage infiltration in the tumor, promoting M2 differentiation when STAC3 is deficient and M1 differentiation under normal conditions (**Figure 8H**). Furthermore, we knocked down STAC3 in the induced macrophages and found that macrophages with low STAC3 expression had increased CD163 expression and decreased CD80 expression. Thus, reduced STAC3 expression in macrophages promotes their differentiation into M2 macrophages. The expression of STAC3 in macrophages also determines their tumor infiltration capacity (**Figure 8H**). Additionally, sh-STAC3 in RAW264.7 cells demonstrated that reduced STAC3 levels lead to decreased phosphorylation of JAK2 and STAT3 proteins, thereby impacting the JAK2/STAT3 signaling pathway in macrophages, which substantiates the critical mechanism by which STAC3 exerts its effects (Supplementary Figure 7C).

*STAC3 impacts the proliferation of KIRC subcutaneous tumors*

In vivo analyses were conducted to evaluate the impact of STAC3 on the proliferation of KIRC through subcutaneous xenograft models in mice. The experimental outcomes demonstrated that STAC3 knockdown significantly inhibited the growth of KIRC subcutaneous tumors (**Figure 9A**). Moreover, growth curve assessments indicated a considerable deceleration in tumor proliferation following STAC3 silencing (**Figure 9B**). Post-extraction, tumor mass measurements revealed that the tumors from the STAC3-depleted group were significantly lighter compared to the controls (**Figure 9C**). Immunohistochemical staining for Ki67 and Cleaved-caspase3 (**Figure 9D**) suggested that loss of STAC3 expression suppressed cellular proliferation and increased apoptosis. The proliferative and apoptotic indices computed post-quantification reinforced the observation that STAC3 depletion curtailed tumor growth and enhanced apoptosis within the tumors (**Figure 9E**, **9F**).

*STAC3-associated drug sensitivity analysis*

Our analysis of STAC3 expression levels and their correlation with sensitivity to a range of FDA-approved pharmacological agents indicates a significant positive relationship between STAC3 expression and the IC50 values for drugs such as Nelarabine, Methylprednisolone, Fluphenazine, ST-3595, Zalcitabine, and Ribavirin. This suggests that tumors with higher STAC3 levels may be more resistant to these drugs. Conversely, increased STAC3 expression correlates with lower IC50 values for Pluripotin, indicating heightened tumor sensitivity to this drug (**Figure 10A**). Through the TCIA database, we downloaded the IPS scores (immunophenoscores) of KIRC patients. We further analyzed the impact of STAC3 expression on the response to anti-cytotoxic T lymphocyte antigen 4 (anti-CTLA-4) and anti-programmed cell death protein 1 (anti-PD-1) antibodies. The results showed that KIRC patients with high STAC3 expression responded better to the combination of anti-PD-1 and anti-CTLA-4 antibodies, as well as to anti-PD-1 alone, whereas STAC3 expression had no significant effect on the response to anti-CTLA-4 alone (**Figure 10B**, **10C**, Supplementary Figure 8). These results imply that patients with low

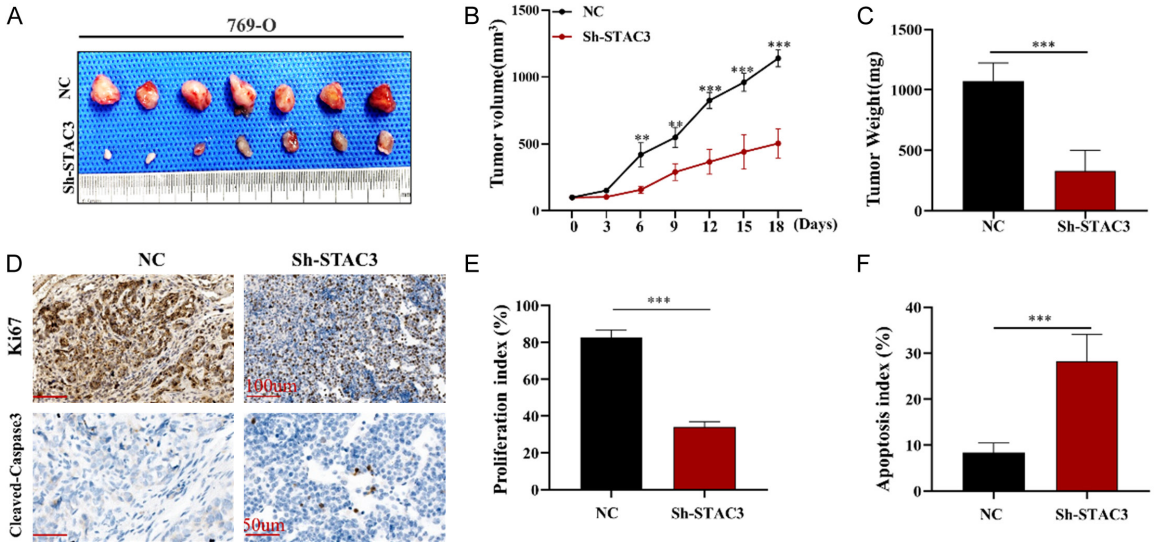


**Figure 9.** Inhibitory effect of STAC3 silencing on subcutaneous tumor growth in mice. A: Visual depiction of the mice's subcutaneous tumors; B: Volumetric evaluation of the tumors in cubic millimeters ($mm^3$); C: Determination of tumor masses in milligrams (mg); D: Microscopic images of tumor slices stained for Ki-67 and cleaved-caspase3 markers; E: Calculation of the proliferation rate, presented as a percentage (%); F: Analysis of apoptosis levels, also shown as a percentage (%). *, $P < 0.05$; **, $P < 0.01$; ***, $P < 0.001$; ****, $P < 0.0001$.

STAC3 expression may respond more favorably to immunotherapy, while those with high expression may derive more benefit from PD-1 inhibitors or a combination of PD1 and CTLA-4 inhibitors.

## Discussion

In this study, we developed a clinical predictive model based on genes associated with calcium ion regulation to assess the prognosis of patients with KIRC. Moreover, the elevated expression of the hub gene STAC3 is closely linked to tumor immunity and poor outcomes in KIRC. Suppression of STAC3 expression was found to inhibit tumor proliferation, migration, invasion, and stemness. Through SSGSEA, single-cell analysis and pseudotime analysis, we confirmed that STAC3 can influence the prognosis of KIRC patients by modulating the tumor immune microenvironment. The regulation of the JAK2/STAT3 signaling pathway by STAC3 may be a critical mechanism by which it exerts its effects. Notably, this discovery was validated in a subcutaneous xenograft model, demonstrating that knockdown of STAC3 inhibits the proliferation of KIRC tumors.

Despite advancements in the 5-year relative survival rates for KIRC, the prognosis for patients, especially those with advanced disease, remains poor [36, 37]. Research by the Memorial Sloan Kettering Cancer Center (MSKCC) has delineated prognostic factors predictive of poor outcomes in KIRC patients. These factors encompass a physical condition index below 80%, serum lactate dehydrogenase levels exceeding 1.5 times the upper normal limit, hemoglobin levels below the normal lower limit, and corrected serum calcium levels above 10 mg/dL [38]. This evidence highlights a marked association between high calcium ion levels and adverse prognosis in KIRC patients, indicating that investigating the impact of calcium ion-regulatory genes on cancer prognosis is imperative for future studies.

Alterations in $Ca^{2+}$ signaling regulatory proteins play a key role in tumorigenesis [39, 40]. $Ca^{2+}$ transport proteins not only affect oncogenic signaling but changes in their expression can initiate the development of specific cancers [41, 42]. Modulating the expression of these $Ca^{2+}$ transport proteins is essential for mitigating tumor growth [43-45]. $Ca^{2+}$ signaling's relationship with specific cell cycle stages significantly impacts cell proliferation, as established in prior research [46]. The impact of $Ca^{2+}$ signaling on proliferation is greatly influenced by the tumor microenvironment [47]. Additionally, $Ca^{2+}$ signaling offers a potential mechanism for the

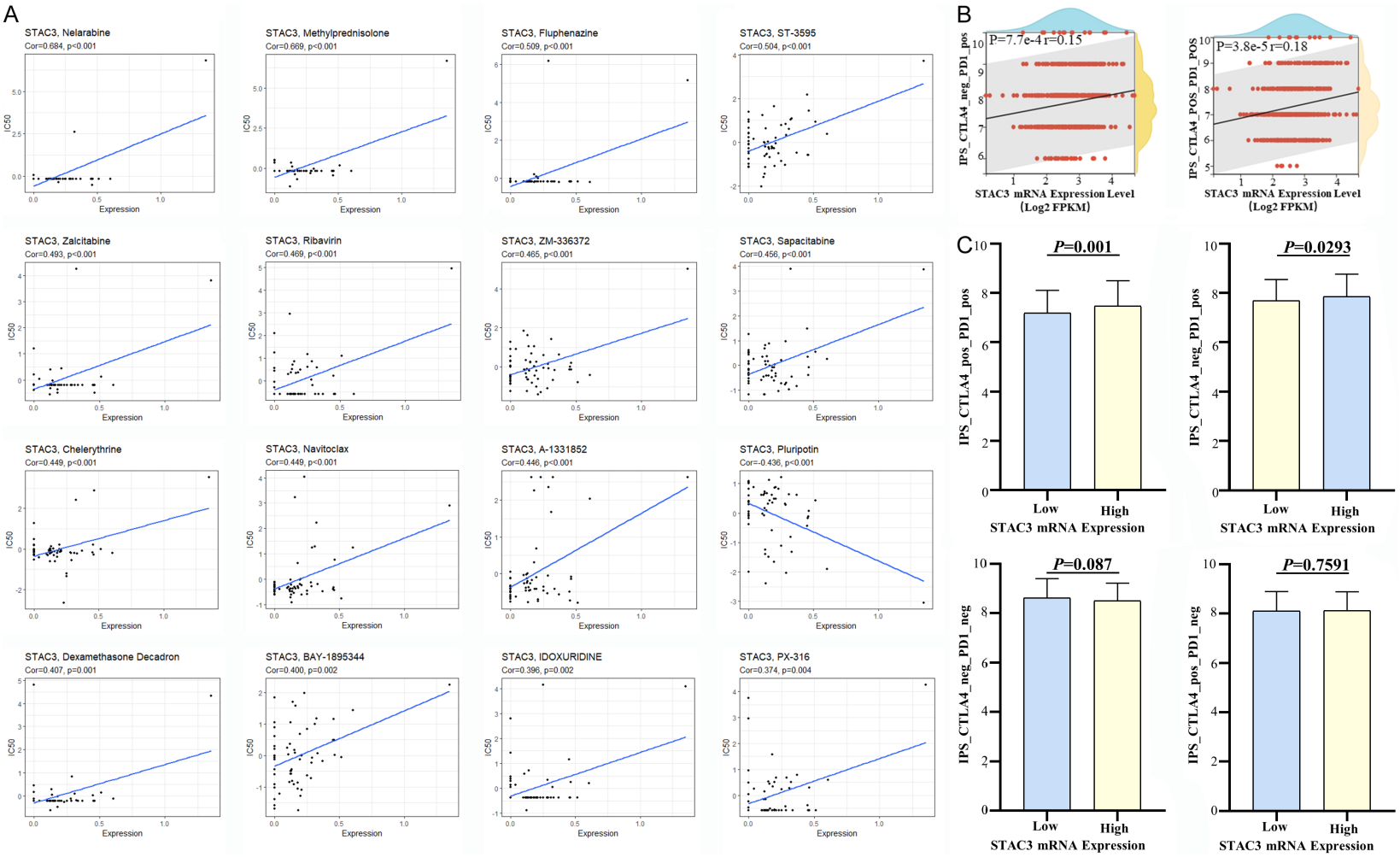


**Figure 10.** Correlation between STAC3 expression and drug sensitivity in KIRC. A: Scatter plots illustrate the correlation between STAC3 expression levels and the half-maximal inhibitory concentration (IC50) for a range of drugs, suggesting a potential impact on therapeutic efficacy; B, C: The expression of STAC3 is associated with the responsiveness of KIRC patients to immunotherapy.

tumor microenvironment to affect cancer cell behavior [11, 47].

This study demonstrates that a clinical prognostic model based on calcium ion-regulating genes can assess the prognosis of tumor patients, where the hub gene STAC3 impacts overall survival, disease-free survival, and disease-specific survival of tumors. STAC3 correlates with tumor malignancy and affects KIRC differentiation, and KIRC tumors with high STAC3 expression tend to be more malignant. Moreover, the expression of STAC3 is significant for tumor proliferation, migration, invasion, and stemness. Meanwhile, intracellular calcium ion concentration was down-regulated after Sh-STAC3. One interaction occurs between the CaV1.1 II-III loop and the SH3 domain of STAC3, and the other interaction is between the C-terminal of CaV1.1 and the linker region of STAC3 [26, 29]. To date, research on STAC3 has been predominantly focused on non-tumor studies [48], with insufficient exploration within the context of cancer. Its role in the progression of renal clear cell carcinoma warrants further investigation. Findings suggest that STAC3 can enrich in tumor immune-related modules and act as a key gene affecting the prognosis of KIRC patients [49]. STAC3, as a macrophage-associated gene, is highly expressed in KIRC tissues and influences the prognosis of tumor patients [18]. Within gene co-expression modules of tumor-infiltrating B lymphocytes (TIL-B), STAC3 serves as a core gene affecting tumor immunity and is highly expressed in KIRC patients, impacting their prognosis [50]. Additionally, STAC3 has been identified as a risk factor in cervical cancer, affecting the prognosis of tumor patients through mechanisms such as m6A methylation [27]. This research innovatively explores the impact of STAC3 on the prognosis of KIRC from the perspective of calcium ion-regulating genes.

Immunotherapy has emerged as the forefront of clinical oncology, providing unparalleled opportunities for the effective management and potential eradication of malignancies once considered intractable [51]. Nonetheless, the efficacy of immunotherapy varies among KIRC patients, underscoring the need for novel therapeutic targets to improve treatment outcomes [1, 20, 52]. However, not all patients with KIRC benefit from immunotherapy, necessitating the identification of new therapeutic targets to enhance treatment efficacy [1, 2, 4, 53]. Recent research has spotlighted differential expression of the STAC3 gene, integral to the muscle excitation-contraction coupling, has been observed in KIRC-associated macrophages, corroborating our observations [18, 49]. Our findings indicate that STAC3 expression significantly influences the infiltration of diverse immune cells, including Tregs, and monocyte macrophages, within this microenvironment. Additionally, we observed that KIRC tissues with high STAC3 expression were associated with increased infiltration of M1 macrophages and regulatory T cells, whereas the infiltration of M2 macrophages was significantly reduced. Single-cell analysis and immunofluorescence staining results revealed that STAC3 is expressed in tumor cells, macrophages, and Tregs, and that STAC3 in both tumor cells and macrophages influences macrophage differentiation. Mechanistically, through cell-cell communication analysis and receptor-ligand pair analysis, we found that STAC3 exerts its effects via the PTN signaling pathway and the ANGPTL4-SDC4 signaling pathway. Further investigation into the underlying mechanisms of STAC3 and how it affects immune cell infiltration and contributes to poor prognosis in tumor patients will be the focus of our next research phase. Evidence suggests that KIRC patients with varying STAC3 expression levels might benefit from immune checkpoint inhibitors, whether used alone or in combination [49]. Our study confirms that patients with low STAC3 expression may respond better to immunotherapy, whereas patients with high expression may benefit more from PD-1 inhibitors or combined PD1 and CTLA-4 inhibitors. However, more validation and mechanistic studies are needed for the use of STAC3 as a molecular marker in cancer immunotherapy.

In essence, our initial analysis supports the development of a prognostic model comprising F2, STAC3, CASQ2, JPH2, MCOLN3, and KCNN3 to accurately forecast KIRC outcomes. Furthermore, STAC3 knockdown has been shown to suppress KIRC cell proliferation, migration, invasion, and in vivo tumor development. The regulation of the immune microenvironment of tumor tissues by STAC3 may be critical for its role. This research aids in the identification of novel prognostic markers for KIRC.

## Acknowledgements

Cancer Research Project of the China Association of Geriatric Health (22992230040; 2022.8.20-2026.8.20) and Research Achievement Transformation and Development Project of Harbin Medical University (22992200-023; 2021.1-2023.12).

## Disclosure of conflict of interest

None.

**Address correspondence to:** Min Guo and Zhifeng Cheng, The Fourth Affiliated Hospital of Harbin Medical University, Harbin 150001, Heilongjiang, China. E-mail: 100886@hrbmu.edu.cn (MG); 002537@hrbmu.edu.cn (ZFC)

## References

[1] Tang C, Xie AX, Liu EM, Kuo F, Kim M, DiNatale RG, Golkaram M, Chen YB, Gupta S, Motzer RJ, Russo P, Coleman J, Carlo MI, Voss MH, Kotecha RR, Lee CH, Tansey W, Schultz N, Hakimi AA and Reznik E. Immunometabolic coevolution defines unique microenvironmental niches in ccRCC. Cell Metab 2023; 35: 1424-1440, e1425.

[2] Krishna C, DiNatale RG, Kuo F, Srivastava RM, Vuong L, Chowell D, Gupta S, Vanderbilt C, Purohit TA, Liu M, Kansler E, Nixon BG, Chen YB, Makarov V, Blum KA, Attalla K, Weng S, Salmans ML, Golkaram M, Liu L, Zhang S, Vijayaraghavan R, Pawlowski T, Reuter V, Carlo MI, Voss MH, Coleman J, Russo P, Motzer RJ, Li MO, Leslie CS, Chan TA and Hakimi AA. Single-cell sequencing links multiregional immune landscapes and tissue-resident T cells in ccRCC to tumor topology and therapy efficacy. Cancer Cell 2021; 39: 662-677, e666.

[3] Clark DJ, Dhanasekaran SM, Petralia F, Pan J, Song X, Hu Y, da Veiga Leprevost F, Reva B, Lih TM, Chang HY, Ma W, Huang C, Ricketts CJ, Chen L, Krek A, Li Y, Rykunov D, Li QK, Chen LS, Ozbek U, Vasaikar S, Wu Y, Yoo S, Chowdhury S, Wyczalkowski MA, Ji J, Schnaubelt M, Kong A, Sethuraman S, Avtonomov DM, Ao M, Colaprico A, Cao S, Cho KC, Kalayci S, Ma S, Liu W, Ruggles K, Calinawan A, Gümüş ZH, Geiszler D, Kawaler E, Teo GC, Wen B, Zhang Y, Keegan S, Li K, Chen F, Edwards N, Pierorazio PM, Chen XS, Pavlovich CP, Hakimi AA, Brominski G, Hsieh JJ, Antczak A, Omelchenko T, Lubinski J, Wiznerowicz M, Linehan WM, Kinsinger CR, Thiagarajan M, Boja ES, Mesri M, Hiltke T, Robles AI, Rodriguez H, Qian J, Fenyö D, Zhang B, Ding L, Schadt E, Chinnaiyan AM, Zhang Z, Omenn GS, Cieslik M, Chan DW, Nesvizhskii AI, Wang P and Zhang H; Clinical Proteomic Tumor Analysis Consortium. Integrated proteogenomic characterization of clear cell renal cell carcinoma. Cell 2019; 179: 964-983, e931.

[4] Pei D, Xu C, Wang D, Shi X, Zhang Y, Liu Y, Guo J, Liu N and Zhu H. A novel prognostic signature associated with the tumor microenvironment in kidney renal clear cell carcinoma. Front Oncol 2022; 12: 912155.

[5] Xu N, Xiao W, Meng X, Li W, Wang X, Zhang X and Yang H. Up-regulation of SLC27A2 suppresses the proliferation and invasion of renal cancer by down-regulating CDK3-mediated EMT. Cell Death Discov 2022; 8: 351.

[6] Siva S, Bressel M, Wood ST, Shaw MG, Loi S, Sandhu SK, Tran B, A Azad A, Lewin JH, Cuff KE, Liu HY, Moon D, Goad J, Wong LM, LimJoon M, Mooi J, Chander S, Murphy DG, Lawrentschuk N and Pryor D. Stereotactic radiotherapy and short-course pembrolizumab for oligometastatic renal cell carcinoma-the RAPPORT trial. Eur Urol 2022; 81: 364-372.

[7] Büttner F, Winter S, Rausch S, Hennenlotter J, Kruck S, Stenzl A, Scharpf M, Fend F, Agaimy A, Hartmann A, Bedke J, Schwab M and Schaeffeler E. Clinical utility of the S3-score for molecular prediction of outcome in non-metastatic and metastatic clear cell renal cell carcinoma. BMC Med 2018; 16: 108.

[8] Brouland JP, Gélébart P, Kovàcs T, Enouf J, Grossmann J and Papp B. The loss of sarco/endoplasmic reticulum calcium transport ATPase 3 expression is an early event during the multistep process of colon carcinogenesis. Am J Pathol 2005; 167: 233-242.

[9] Tsavaler L, Shapero MH, Morkowski S and Laus R. Trp-p8, a novel prostate-specific gene, is up-regulated in prostate cancer and other malignancies and shares high homology with transient receptor potential calcium channel proteins. Cancer Res 2001; 61: 3760-3769.

[10] Dhennin-Duthille I, Gautier M, Faouzi M, Guilbert A, Brevet M, Vaudry D, Ahidouch A, Sevestre H and Ouadid-Ahidouch H. High expression of transient receptor potential channels in human breast cancer epithelial cells and tissues: correlation with pathological parameters. Cell Physiol Biochem 2011; 28: 813-822.

[11] Monteith GR, Prevarskaya N and Roberts-Thomson SJ. The calcium-cancer signalling nexus. Nat Rev Cancer 2017; 17: 367-380.

[12] Lee SS, Kwon SJ, Lee DE, Lee S, Baird A, Park SY, Dolan J and George S. Modeling of prognostication and differential genomic expression in the tumor microenvironment of clear

cell renal cell carcinoma. J Clin Oncol 2019; 37 Suppl: 557.
[13] Obradovic A, Chowdhury N, Haake SM, Ager C, Wang V, Vlahos L, Guo XV, Aggen DH, Rathmell WK, Jonasch E, Johnson JE, Roth M, Beckermann KE, Rini BI, McKiernan J, Califano A and Drake CG. Single-cell protein activity analysis identifies recurrence-associated renal tumor macrophages. Cell 2021; 184: 2988-3005, e16.
[14] Bond KH, Chiba T, Wynne KPH, Vary CPH, Sims-Lucas S, Coburn JM and Oxburgh L. The extracellular matrix environment of clear cell renal cell carcinoma determines cancer associated fibroblast growth. Cancers (Basel) 2021; 13: 5873.
[15] Wang M, Song Q, Song Z and Xie Y. Development of an immune prognostic model for clear cell renal cell carcinoma based on tumor microenvironment. Horm Metab Res 2023; 55: 402-412.
[16] Bruni D, Angell HK and Galon J. The immune contexture and Immunoscore in cancer prognosis and therapeutic efficacy. Nat Rev Cancer 2020; 20: 662-680.
[17] Yang C, Yu T and Lin Q. A signature based on chromatin regulation and tumor microenvironment infiltration in clear cell renal cell carcinoma. Epigenomics 2022; 14: 995-1013.
[18] Dong K, Chen W, Pan X, Wang H, Sun Y, Qian C, Chen W, Wang C, Yang F and Cui X. FCER1G positively relates to macrophage infiltration in clear cell renal cell carcinoma and contributes to unfavorable prognosis by regulating tumor immunity. BMC Cancer 2022; 22: 140.
[19] Fridman WH, Zitvogel L, Sautès-Fridman C and Kroemer G. The immune contexture in cancer prognosis and treatment. Nat Rev Clin Oncol 2017; 14: 717-734.
[20] Xu H, Zheng X, Zhang S, Yi X, Zhang T, Wei Q, Li H and Ai J. Tumor antigens and immune subtypes guided mRNA vaccine development for kidney renal clear cell carcinoma. Mol Cancer 2021; 20: 159.
[21] Bi X, Lu Y, Bi X and Luo Z. Hot clear cell renal cell carcinoma immune status: illusion or reality? J Clin Oncol 2021; 39 Suppl: e16575.
[22] Graham J, Wells C, Dudani S, Gan CL, Donskov F, Lee JL, Kollmannsberger CK, Pal S, Beuselinck B, Hansen AR, North SA, Bjarnason GA, Agarwal N, Kanesvaran R, Wood L, Hotte SJ, McKay R, Choueiri TK and Chin Heng DY. Effectiveness of first-line immune checkpoint inhibitors (ICI) in advanced non-clear cell renal cell carcinoma (ccRCC). J Clin Oncol 2021; 39 Suppl: 316.
[23] Rufenach B, Christy D, Flucher BE, Bui JM, Gsponer J, Campiglio M and Van Petegem F. Multiple sequence variants in STAC3 affect interactions with CaV1.1 and excitation-contraction coupling. Structure 2020; 28: 922-932, e5.
[24] Campiglio M, Kaplan MM and Flucher BE. STAC3 incorporation into skeletal muscle triads occurs independent of the dihydropyridine receptor. J Cell Physiol 2018; 233: 9045-9051.
[25] Török E, Tuinte WE and Campiglio M. Identifying the STAC3/CaV1.1 interactions responsible for CaV1.1 expression in skeletal muscle. Biophys J 2023; 122: 376a.
[26] Niu J, Ben Johny M, Yue D and Inoue T. Calmodulin and Stac3 enhance functional expression of Ca V 1.1. Biophys J 2017; 112: 108a.
[27] Wang Y, Mao Y, Wang C, Jiang X, Tang Q, Wang L, Zhu J and Zhao M. RNA methylation-related genes of m6A, m5C, and m1A predict prognosis and immunotherapy response in cervical cancer. Ann Med 2023; 55: 2190618.
[28] Tuinte WE, Török E, Mahlknecht I, Tuluc P, Flucher BE and Campiglio M. STAC3 determines the slow activation kinetics of Ca V 1.1 currents and inhibits its voltage-dependent inactivation. J Cell Physiol 2022; 237: 4197-4214.
[29] Campiglio M and Flucher BE. STAC3 stably interacts through its C1 domain with Ca V 1.1 in skeletal muscle triads. Sci Rep 2017; 7: 41003.
[30] Cong X, Doering J, Mazala DA, Chin ER, Grange RW and Jiang H. The SH3 and cysteine-rich domain 3 (Stac3) gene is important to growth, fiber composition, and calcium release from the sarcoplasmic reticulum in postnatal skeletal muscle. Skelet Muscle 2016; 6: 17.
[31] Liu A, Li F, Wang B, Yang L, Xing H, Su C, Gao L, Zhao M and Luo L. Prognostic and immunological significance of calcium-related gene signatures in renal clear cell carcinoma. Front Pharmacol 2022; 13: 1055841.
[32] Beckermann KE and Rini BI. Sequencing checkpoint inhibitor therapy in renal cell carcinoma. Lancet 2023; 402: 160-161.
[33] Huang B, Lang X and Li X. The role of IL-6/JAK2/STAT3 signaling pathway in cancers. Front Oncol 2022; 12: 1023177.
[34] Shi Y, Ping YF, Zhou W, He ZC, Chen C, Bian BS, Zhang L, Chen L, Lan X, Zhang XC, Zhou K, Liu Q, Long H, Fu TW, Zhang XN, Cao MF, Huang Z, Fang X, Wang X, Feng H, Yao XH, Yu SC, Cui YH, Zhang X, Rich JN, Bao S and Bian XW. Tumour-associated macrophages secrete pleiotrophin to promote PTPRZ1 signalling in glioblastoma stem cells for tumour growth. Nat Commun 2017; 8: 15080.
[35] Yang M, Wang B, Yin Y, Ma X, Tang L, Zhang Y, Fan Q, Yin T and Wang Y. PTN-PTPRZ1 signal-

ing axis blocking mediates tumor microenvironment remodeling for enhanced glioblastoma treatment. J Control Release 2023; 353: 63-76.
[36] Barata PC and Rini BI. Treatment of renal cell carcinoma: current status and future directions. CA Cancer J Clin 2017; 67: 507-524.
[37] Liang F. Optimising first-line treatment for metastatic renal cell carcinoma. Lancet 2020; 395: e8.
[38] Motzer RJ, Mazumdar M, Bacik J, Berg W, Amsterdam A and Ferrara J. Survival and prognostic stratification of 670 patients with advanced renal cell carcinoma. J Clin Oncol 1999; 17: 2530-2540.
[39] Monteith GR, Davis FM and Roberts-Thomson SJ. Calcium channels and pumps in cancer: changes and consequences. J Biol Chem 2012; 287: 31666-31673.
[40] Prevarskaya N, Ouadid-Ahidouch H, Skryma R and Shuba Y. Remodelling of Ca2+ transport in cancer: how it contributes to cancer hallmarks? Philos Trans R Soc Lond B Biol Sci 2014; 369: 20130097.
[41] Roderick HL and Cook SJ. Ca2+ signalling checkpoints in cancer: remodelling Ca2+ for cancer cell proliferation and survival. Nat Rev Cancer 2008; 8: 361-375.
[42] Prevarskaya N, Skryma R and Shuba Y. Calcium in tumour metastasis: new roles for known actors. Nat Rev Cancer 2011; 11: 609-618.
[43] Khan HY, Mpilla GB, Sexton R, Viswanadha S, Penmetsa KV, Aboukameel A, Diab M, Kamgar M, Al-Hallak MN, Szlaczky M, Tesfaye A, Kim S, Philip PA, Mohammad RM and Azmi AS. Calcium release-activated calcium (CRAC) channel inhibition suppresses pancreatic ductal adenocarcinoma cell proliferation and patient-derived tumor growth. Cancers (Basel) 2020; 12: 750.
[44] Fang Y, Liu L, Liu S, Hu L, Cai W, Wan X, Liu D, He Y and Zhu Z. Calcium-sensing receptor promotes tumor proliferation and migration in human intrahepatic cholangiocarcinoma by targeting ERK signaling pathway. Eur J Pharmacol 2020; 872: 172915.
[45] Pinto MC, Kihara AH, Goulart VA, Tonelli FM, Gomes KN, Ulrich H and Resende RR. Calcium signaling and cell proliferation. Cell Signal 2015; 27: 2139-2149.
[46] Sée V, Rajala NK, Spiller DG and White MR. Calcium-dependent regulation of the cell cycle via a novel MAPK--NF-kappaB pathway in Swiss 3T3 cells. J Cell Biol 2004; 166: 661-672.
[47] Bissell MJ and Hines WC. Why don't we get more cancer? A proposed role of the microenvironment in restraining cancer progression. Nat Med 2011; 17: 320-329.
[48] Williams SP, Hernández Rodríguez MY, Cass B, Ali-Dinar T and ElMallah MK. Pulmonary manifestations of STAC3 disorder: a case series. Pediatr Pulmonol 2024; 59: 794-797.
[49] Qu H, Mao M, Wang K, Mu Z and Hu B. Knockdown of ADAM8 inhibits the proliferation, migration, invasion, and tumorigenesis of renal clear cell carcinoma cells to enhance the immunotherapy efficacy. Transl Res 2024; 266: 32-48.
[50] Yue Y, Cai X, Lu C, Sechi LA, Solla P and Li S. Unraveling the prognostic significance and molecular characteristics of tumor-infiltrating B lymphocytes in clear cell renal cell carcinoma through a comprehensive bioinformatics analysis. Front Immunol 2023; 14: 1238312.
[51] Xia H, Green DR and Zou W. Autophagy in tumour immunity and therapy. Nat Rev Cancer 2021; 21: 281-297.
[52] Li J, Liu C, Su H, Dong H, Wang Z, Wang Y, Zhao P, Zhang C, Zhao Y and Ma X. Integrative analysis of LAG3 immune signature and identification of a LAG3-related genes prognostic signature in kidney renal clear cell carcinoma. Aging (Albany NY) 2024; 16: 2161-2180.
[53] Cai Z, He Y, Yu Z, Hu J, Xiao Z, Zu X, Li Z and Li H. Cuproptosis-related modification patterns depict the tumor microenvironment, precision immunotherapy, and prognosis of kidney renal clear cell carcinoma. Front Immunol 2022; 13: 933241.

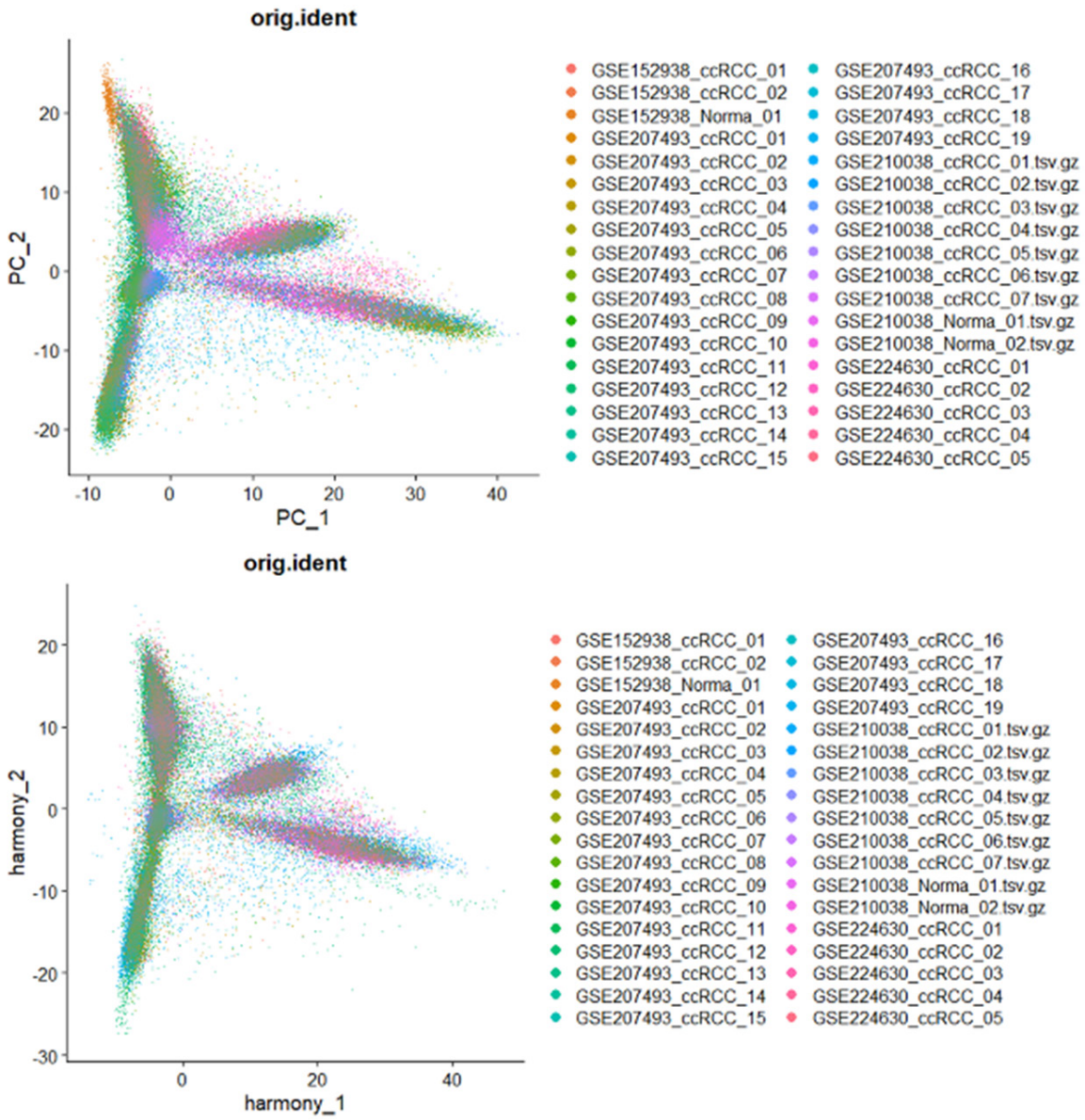


**Supplementary Figure 1.** Eliminate batch effects in sample data.

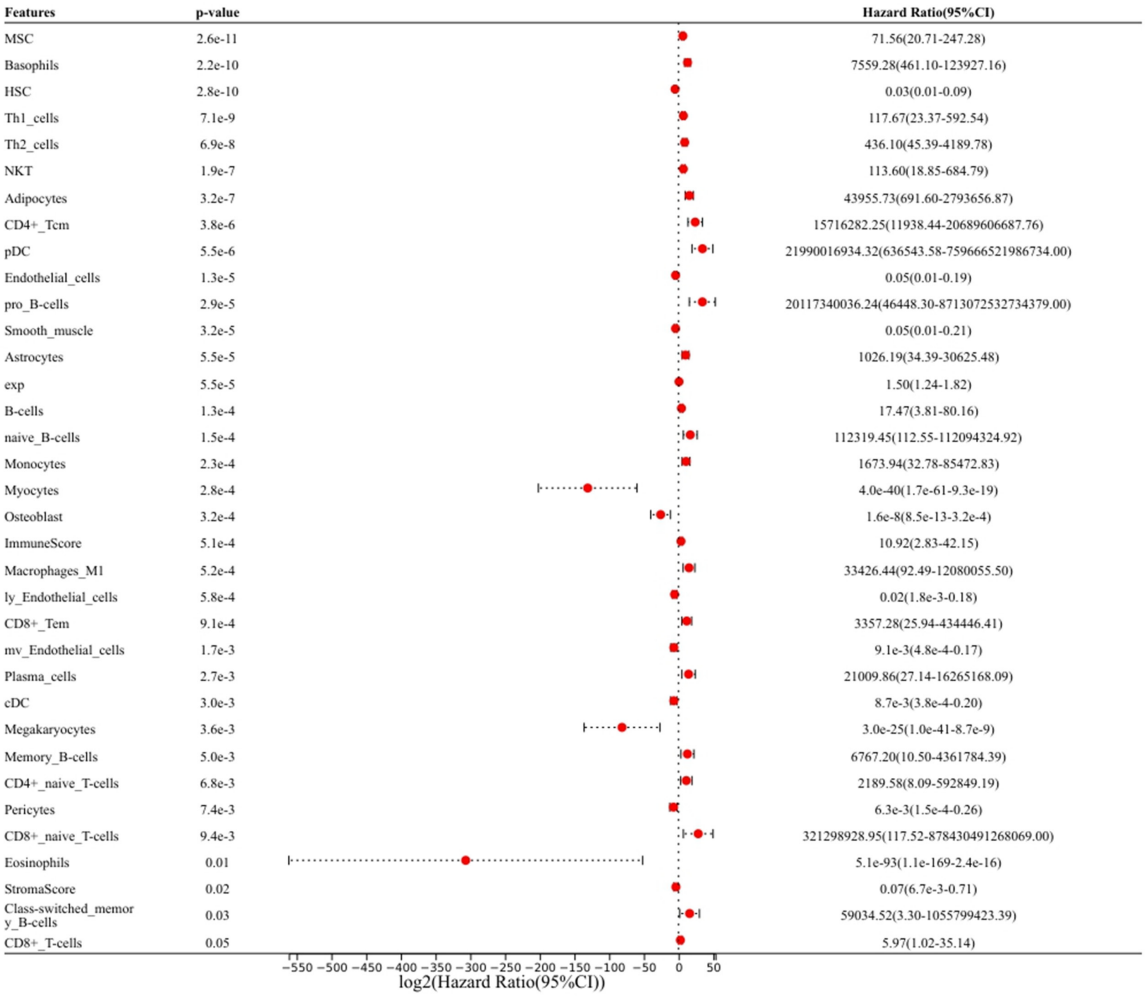


**Supplementary Figure 2.** Impact of immune cell populations on clinical outcomes in KIRC.

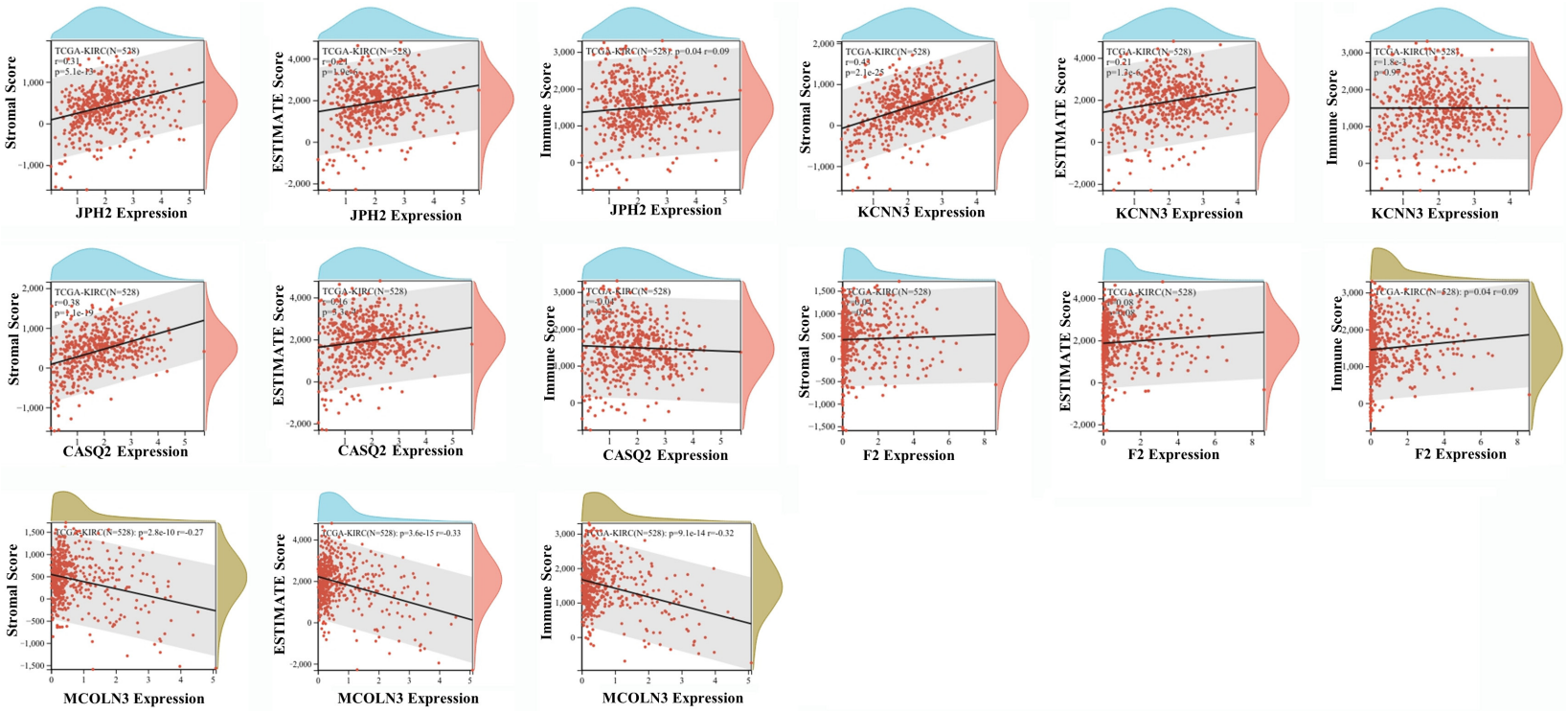


**Supplementary Figure 3.** Correlation analysis of hub genes (JPH2, CASQ2, MCOLN3, KCNN3, F2) with tumor stromal score, ESTIMATE score, and immune score. *, P<0.05; **, P<0.01; ***, P<0.001; ****, P<0.0001.

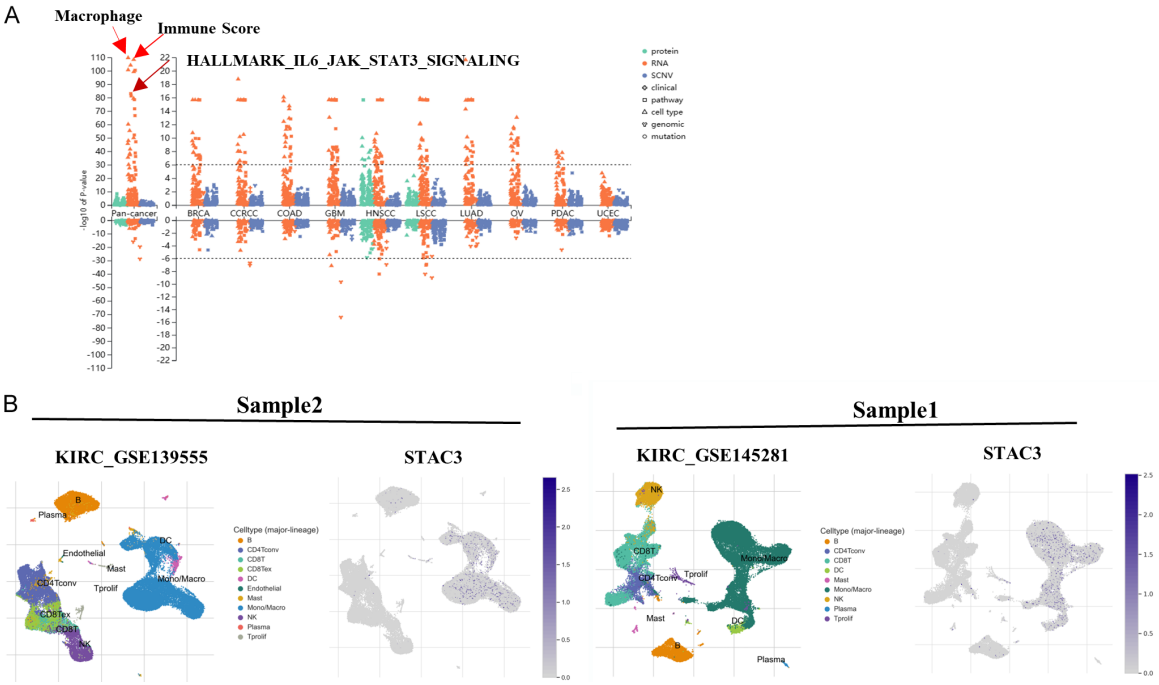


**Supplementary Figure 4.** Exploring the mechanism of STAC3's impact on tumor immunity. A: Elevated STAC3 expression across various tumors correlates with increased macrophage infiltration, higher Immune Score, and activation of the HALLMARK IL-6 JAK-STAT3 signaling pathway. B: Pronounced expression of STAC3 in monocytes/macrophages within tumor tissues suggests a role in immune cell function.

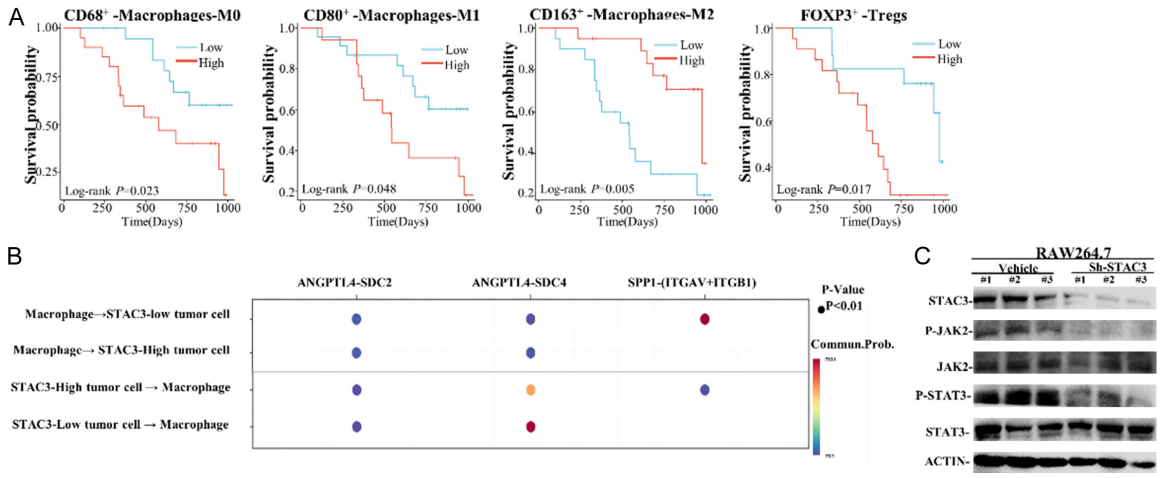


**Supplementary Figure 5.** Mechanism of the effect of STAC3 on tumor immune infiltration. A: CD68+ M0 macrophages, CD80+ M1 macrophages, CD163+ M2 macrophages, and Foxp3+ Tregs significantly impact the survival of KIRC patients. B: Analysis of receptor-ligand pairs between tumor cells with high and low STAC3 expression and macrophages. C: Inhibition of STAC3 reduces JAK2/STAT3 signaling pathway activation in macrophages.

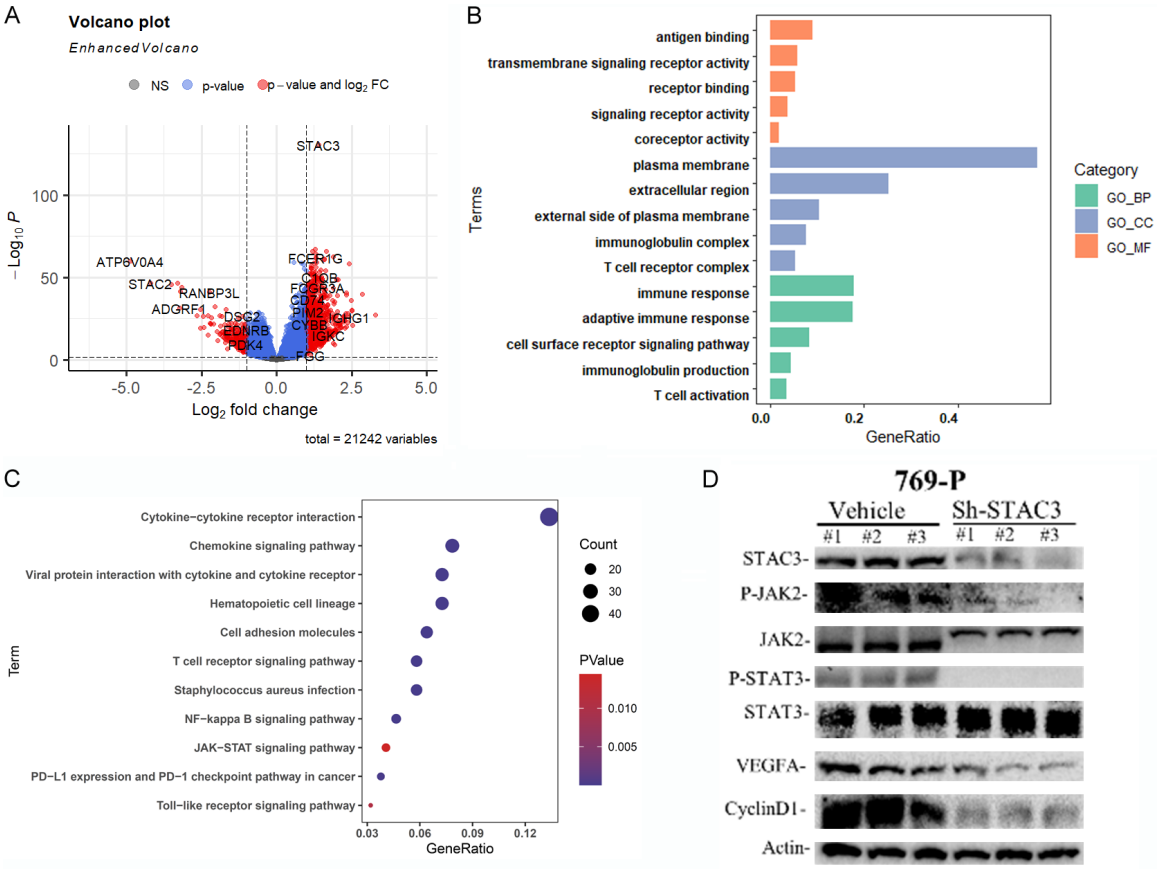


**Supplementary Figure 6.** Investigation into the mechanisms by which STAC3 affects tumor cell proliferation and invasion. A: Differentially expressed genes associated with STAC3 expression. B: GO enrichment analysis of differentially expressed genes. C: KEGG pathway enrichment analysis of differentially expressed genes. D: STAC3 regulation of the JAK2/STAT3 signaling pathway in tumor cells.

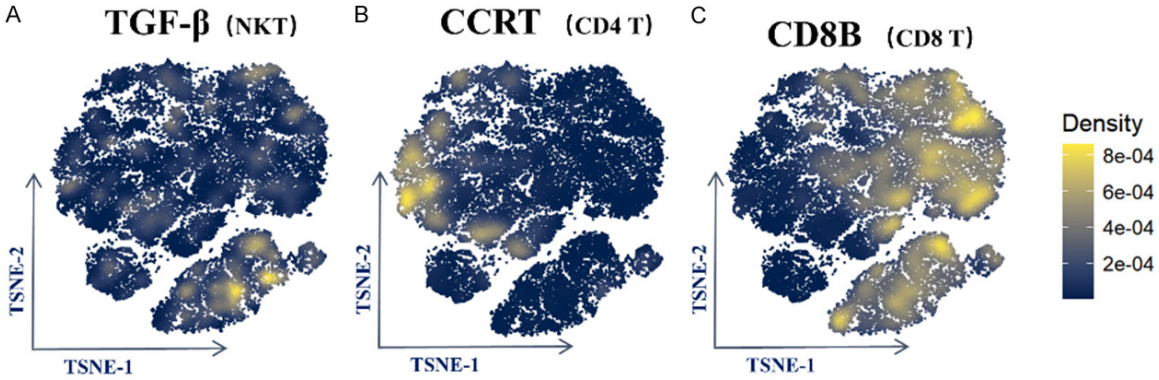


**Supplementary Figure 7.** TGF-β, CCRT, CD8B expression on NKT cells, CD4 T cells and CD8 T cells.

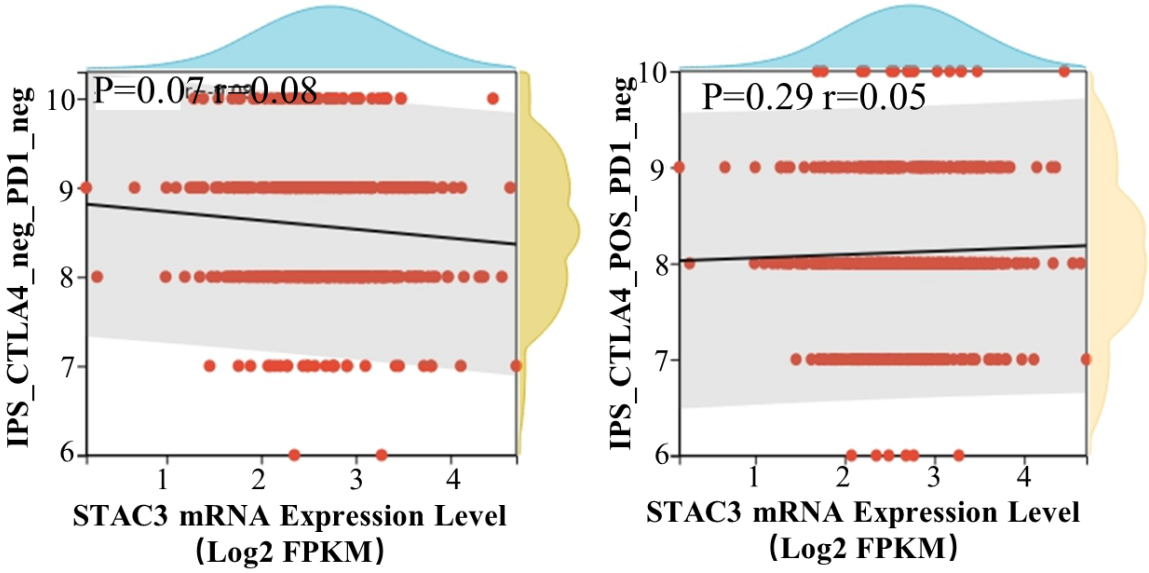


**Supplementary Figure 8.** Correlation analysis between STAC3 expression and IPS scores of patients undergoing different immunotherapy approaches (CTLA4_neg_PD1_neg, CTLA4_pos_PD1_neg).